Title	Recent advances in vanadium-based cathode materials for rechargeable zinc ion batteries
Author(s)	Yao Zhang, Edison Huixiang Ang, Khang Ngoc Dinh, Kun Rui, Huijuan Lin, Jixin Zhu, and Qingyu Yan
Source	*Materials Chemistry Frontiers,* (2020)
Published by	Royal Society of Chemistry

The final publication is also available at https://doi.org/10.1039/D0QM00577K

MATERIALS CHEMISTRY
FRONTIERS

Accepted Manuscript

This article can be cited before page numbers have been issued, to do this please use: Y. Zhang, H. Ang, K. N. Dinh, K. Rui, H. Lin, J. Zhu and Q. Yan, *Mater. Chem. Front.*, 2020, DOI: 10.1039/D0QM00577K.

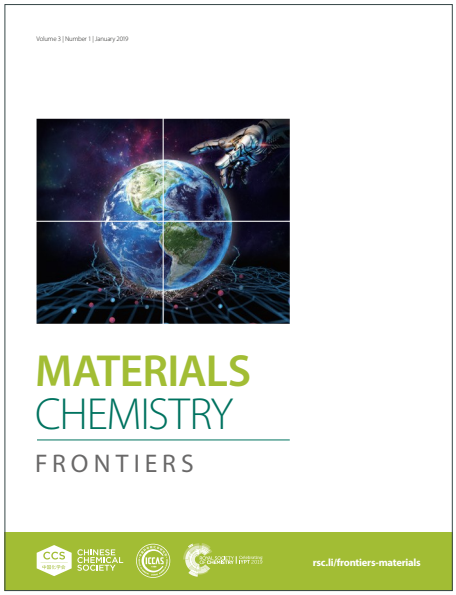

View Article Online
DOI: 10.1039/D0QM00577K

Materials Chemistry Frontiers

Review

Recent Advances in Vanadium-Based Cathode Materials for Rechargeable Zinc Ion Batteries

Yao Zhang,[‡a] Edison Huixiang Ang,[‡b] Khang Ngoc Dinh,[c] Kun Rui,[a] Huijuan Lin,[a] Jixin Zhu,*[a] and Qingyu Yan*[c]

Received 00th January 20xx,
Accepted 00th January 20xx

DOI: 10.1039/x0xx00000x

www.rsc.org/

The fast depletion of lithium resources has led to active research works on other emerging electrochemical energy storage systems. Among those, many works have focused on the development of cathode materials of zinc ion batteries for even higher energy efficiency, outstanding rate capability, remarkable power density, and longer lifetime. Vanadium-based nanomaterials show fast ion diffusion and excellent reversible capacity because of their rich valence state of vanadium, facile distortion of V-O polyhedrons, and tunable chemical composition, offering great opportunities for developing emerging energy storage technologies. This article systematically reviews vanadium-based nanomaterials in the cathode materials for zinc ion batteries, aiming to present a comprehensive discussion. Herein, we group vanadium-based cathode materials into three categories including vanadium oxides, vanadates, and vanadium phosphates. Cathode electrochemical performance, improvement strategy, structural stability, and zinc storage mechanism are reviewed in detail. Lastly, the existing bottlenecks and prospects are provided for further progressive research.

1. Introduction

The looming energy crisis and environmental concerns have promoted the transformation of the world energy landscape to sustainable energy development.[1-6] As efficient means of energy storage, batteries are commonly used for e-mobility, portable electronics, and micro-grids. Among all, lithium ion batteries (LIBs) are widely used due to their high energy density, reasonable lifespan.[7-10] Nevertheless, the limited lithium resources, increasing cost, and safety concerns encourage researchers to put efforts on other metal ion battery chemistries of mono- (K, Na) and multivalent (Mg, Ca, Zn, Al) ions.[11-18]

As one of the most promising energy storage solutions for micro-grids, rechargeable zinc ion batteries (ZIBs) can bring the intermittent renewable energy to rural areas.[19, 20] The benefits of ZIBs includes abundant natural resources, environmental friendliness, low oxidation-reduction potential of Zn (-0.76 V), and high theoretical capacity (820 mAh g^{-1}).[21, 22] It is expected that ZIBs can bear a higher energy density than those of other alkali metal ion batteries through realizing a broad voltage window during reaction. The ZIBs cathode material has less deintercalated ions at the same discharge capacity; thus, crystal structure is preserved, ensuring good electrode stability. The research on secondary ZIBs started in 1988 when Shoji *et al.* demonstrated a rechargeable ZIB using zinc flakes and manganese dioxide as the anode and cathode materials, respectively, and neutral zinc sulfate aqueous solution as the electrolyte.[23] The MnO_2 exhibits large and stable tunnels, making it easier for reversible injection and removal of Zn^{2+} ions. Since then, the research of ZIBs focuses mainly on nanostructured cathode materials. Apart from different crystal forms of manganese-based oxides, other promising materials were also explored for ZIBs (Prussian blue analogs and some organic materials). These materials often have their own shortcomings, such as unsatisfactory rate performance of manganese dioxide and low capacity of Prussian blue analogues.

Vanadium-based compounds have recently become a hot research topic for the ZIBs, thanks to the versatile V-O octahedra structure and multiple oxidation states of vanadium.[24] The degree of occupancy in the d-orbital can influence the magnitude of the structural change. In octahedral configuration, a small volume change will occur when nonbonding orbitals are filled. However, if antibonding orbitals are filled, the volume will suffer a huge extension. As one of the

[a] Key Laboratory of Flexible Electronics (KLOFE) & Institute of Advanced Materials (IAM), Jiangsu National Synergetic Innovation Center for Advanced Materials (SICAM), Nanjing Tech University (NanjingTech), 30 South Puzhu Road, Nanjing 211816, China
[b] Natural Sciences and Science Education, National Institute of Education, Nanyang Technological University, 637616, Singapore
[c] School of Materials Science and Engineering, Nanyang Technological University, 50 Nanyang Avenue, Singapore 639798, Singapore
‡ These authors contributed equally to this work.

Jixin Zhu

Jixin Zhu is currently a full Professor at the Institute of Advanced Materials, Nanjing Tech University. In 2012, he received his Ph.D. degree from Nanyang Technological University and then worked as a postdoctoral fellow in TUM CREATE from 2012 to 2014. After that, he moved to Max Planck Institute of Colloids and Interfaces as a postdoctoral fellow. He was selected as Clarivate Analytics "Highly Cited Researcher". His research topics mainly include advanced functional materials for energy storage and conversion, flexible electronics devices applications.

Qingyu Yan

Qingyu Yan is currently a professor in School of Materials Science and Engineering in Nanyang Technology University. He reveived his Ph.D from Materials Science and Engineering Department of State University of New York at Stony Brook. After that, he worked as a postdoctoral research associate in the department of Rensselaer Polytechnic Institute. Then he joined School of Materials Science and Engineering of Nanyang Technological University as an assistant professor in early 2008 and became a professor in 2018. His research interests focus on advanced electrode materials for energy storage devices and cost-effective electrocatalysts.

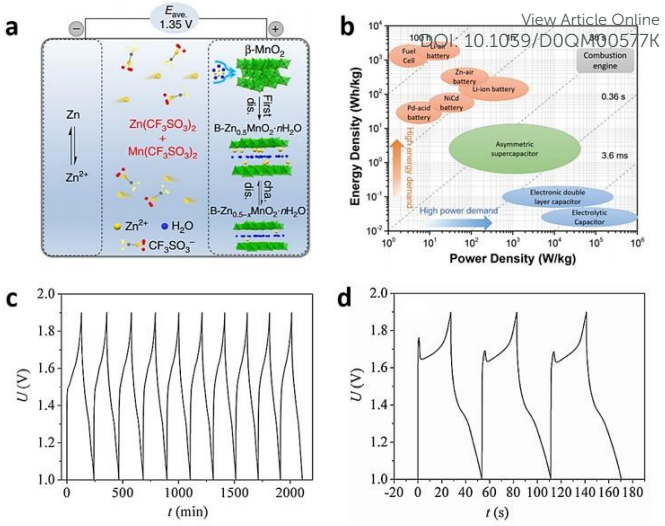

Fig. 1 (a) Schematic illustration for interior constitute of rechargeable Zn-MnO_2 energy storage system. Replicated with permission from ref. 30. Copyright 2015 Springer Nature. (b) Comparison of Ragone plots among various energy storage technologies. Reprinted with permission from ref. 31. Copyright 2018 American Chemical Society. (c-d) *V-t* curves of ZIBs using MnO_2 as cathode at 100 mA g^{-1} and 8000 mA g^{-1}, respectively. Reprinted with permission from ref. 35. Copyright 2012 WILEY-VCH.

early transition metals, vanadium will bear a small volume change due to the presence of many unoccupied nonbonding orbitals. Moreover, the different oxidation states of vanadium allow higher degree of structural changes and greater functional flexibility when introducing multivalent cations into vanadium-based compounds.[25, 26] Vanadium could facilitate realizing local electroneutrality by altering two or more oxidation states to stabilize the crystal structure and optimizing the multivalent mechanism of cation diffusion. Those peculiar vanadium properties make it a suitable choice for the use of cathode materials for ZIBs.[27, 28]

In this minireview, we present an analysis on the latest progresses of vanadium-based nanomaterials for ZIBs to provide necessary comprehension for the further evolution of nanostructured vanadium-based materials. In addition to electrochemical properties of various vanadium related compounds, the dynamic mechanism of intercalation between multivalent cations and materials are also described extensively. In the end, challenges and prospects for ZIBs in the above areas are discussed.

2. The overview of zinc ion batteries

Zinc-based batteries have been mainly used as primary batteries, which raised the problem with regards to waste management and environmental pollution. The zinc-based battery industry should conform with the current energy efficiency and environmental policies if such large amounts of primary batteries can be converted to secondary batteries. Zinc-based primary batteries mainly include zinc-manganese (Zn/MnO_2) batteries, zinc-silver (Zn/AgO) batteries, zinc-nickel (Zn/NiOOH) batteries, and zinc-air (Zn/Ai) batteries. In the 1970s, rechargeable zinc-manganese dioxide batteries were first put on the market. This is an extension of alkaline battery technology, but it has the shortcomings of unstable cycling performance, short cycling lifespan, and the inability to charge/discharge at large currents. Therefore, to further improve the rechargeability, cycling stability, and discharge performance at a high current density, new rechargeable ZIBs are highly desirable.

2.1 Concept and principle of zinc ion batteries

Zinc ion batteries are mainly secondary batteries. Cairns *et al.* described a divalent ion energy storage system for α-MnO_2, and further extended into cathode materials for ZIB in neutral electrolyte systems.[29] ZIBs usually employ large-tunnel α-MnO_2 or layered vanadium oxides as cathode materials, metallic zinc as the anode, and a neutral or weakly acidic aqueous solution containing Zn^{2+} as the electrolyte. During operation, cathode material undergoes a structural change, *i.e.* transforming into a new phase containing zinc. Once fully discharge, the new phase and the original phase can coexist. The electrochemical principle of zinc ion battery is depicted in **Fig. 1**a.[30] Taking the manganese oxide cathode material as an example, when being charged, Zn^{2+} is extracted from the cathode MnO_2 tunnel structure and then deposited on the surface of the anode zinc. During discharge, the zinc anode loses electrons to form zinc

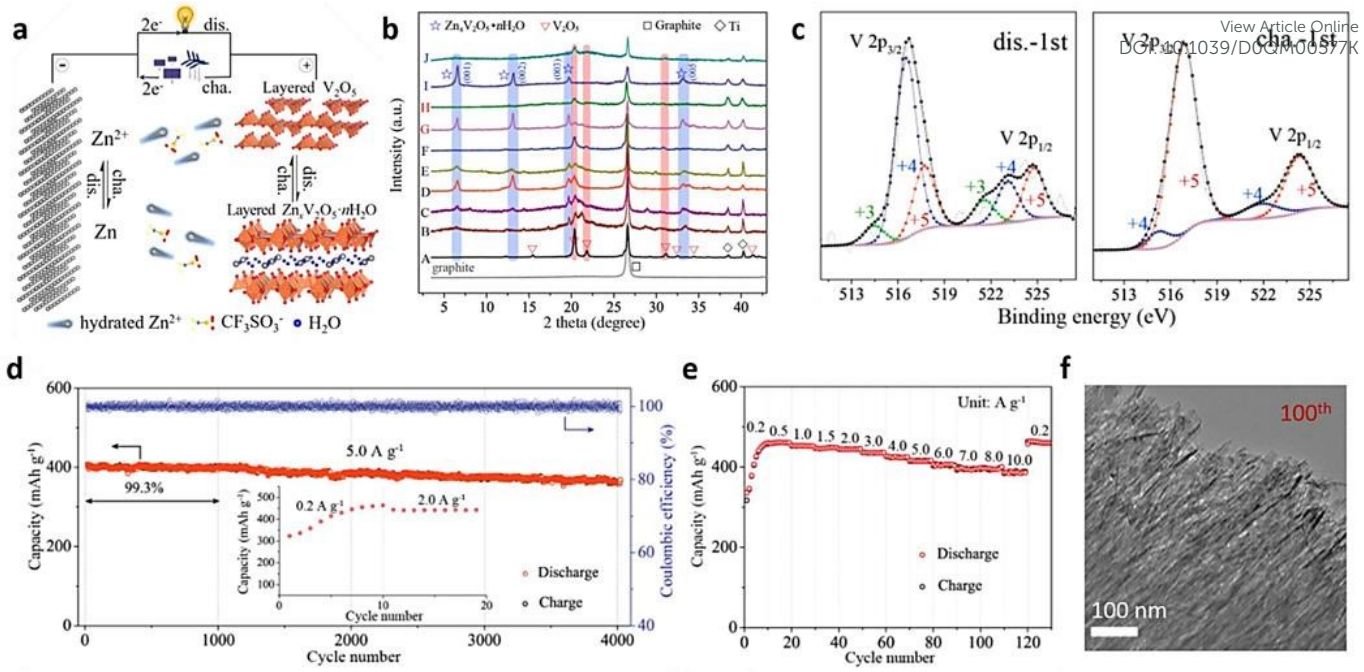

Fig. 2 (a) The schematic illustration for a typical rechargeable Zn-V_2O_5 battery system. (b) Ex-situ XRD patterns of V_2O_5 cathode at selected status during charging and discharging process. (c) Ex-situ XPS analysis of V 2p at completely discharged and charged state of the first cycle. (d) Cycling stability of V_2O_5 cathode 5.0 A g^{-1}. (e) Rate-capacity performance of V_2O_5 at various current density. (f) TEM image of V_2O_5 electrode after 100 cycles. Reproduced with permission from ref. 41. Copyright 2018 American Chemical Society.

ions which is then embedded in MnO_2 tunnel. Therefore, the ZIB can be visually compared to a "rocking chair battery", *i.e.* zinc ions run back and forth at both ends of the rocking chair, that is, the positive and negative electrodes of the battery.

2.2 The advantages of zinc ion batteries

Zinc ion batteries exhibit superior electrochemical performances compared to others. In general, the following are the most noticeable:

i). High power density and high energy density. Current literature has reported ZIBs with high energy density and power density of up to 320 Wh kg^{-1} and 12 kW kg^{-1}, respectively, which is much higher than the existing alkali metal ion batteries, nickel-cadmium batteries, supercapacitors, lead-acid batteries (Fig. 1b).[31-34] Furthermore, the commercially available batteries have not been able to provide both high power density and high energy density simultaneously. And this is where ZIBs can really come in and make a difference.

ii). Superior rate performance. As shown in Fig. 1c and Fig. 1d, ZIBs with MnO_2 cathode is able to discharge at a current density of 100 mA g^{-1}. Noticeably, when a large current of 8000 mA g^{-1} is applied, the battery can complete a charging process in only 30 s.[35]

iii). Low manufacturing and material cost. ZIBs can be assembled in ambient air, which saves assembly costs to a considerable extent when compared to lithium or sodium batteries. Meanwhile, zinc metal is rich in resources and inexpensive (<$1/lb compared to ~13/lb of Co). This potential low cost of zinc ion battery will reshape the battery industry.

iv). Environmentally friendly and safe. The electrolyte of the zinc ion battery uses near-neutral aqueous solution of zinc sulfate and zinc acetate (pH between 5~7). Zinc metal and its inorganic salts are non-toxic, recyclable, and no pollutants will be produced in the production of batteries.

2.3. The anode material of zinc ion batteries

Metallic zinc plays a crucial part as anode material in zinc ion batteries. Zinc crystals exhibit a close-packed hexagonal structure, with deformation and anisotropy characteristics. Zinc is an amphoteric metal with relatively active chemical properties. It can quickly dissolve near its equilibrium potential and generate divalent ions. The dissolved product in acidic solution is Zn^{2+}, while the main dissolved product in alkaline solution is tetrahedron $Zn(OH)_4^{2-}$. The standard reduction potential of zinc compared to other metals indicates its great potentials as electrode material. As battery anode, zinc has numerous advantages including rich resources, low-cost, low toxicity, good conductivity, high hydrogen evolution overpotential, and high energy density.

3. Vanadium-based cathode materials for zinc ion batteries

Vanadium-based compounds, especially vanadium-based oxides, have been extensively applied as zinc storage materials on account of their low cost, abundant resources, and multiple oxidation states (V^{2+} to V^{5+}). Due to the diversity of the V-O coordination polyhedron structure, there are many types of vanadium-based oxides. As the valence state of the vanadium changes, the structure of the V and O-coordinated polyhedron also changes; hence, the intercalation/deintercalation of the multivalent ions will not destroy the structure of the vanadium oxide. In 1998, V_2O_5 aerogel was reported for the first time to

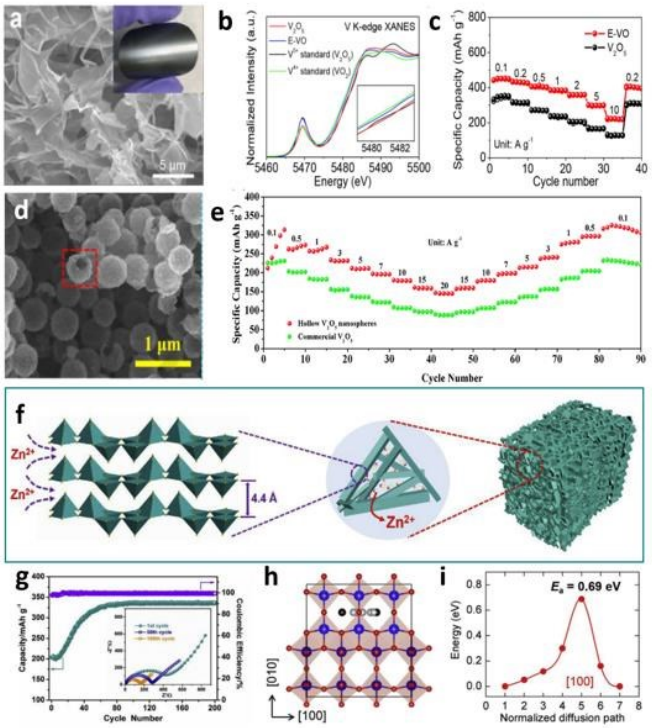

Fig. 3 (a) SEM image of E-VO electrode. (b) Normalized V K-edge XANES for E-VO, V_2O_5, standard V^{5+} and standard V^{4+}. (c) The rate performances of E-VO electrode and V_2O_5 electrode. Reprinted with permission from ref. 66. Copyright 2019 Elsevier. (d) The SEM image of hollow V_2O_5 nanosphere. (e) The rate performances of hollow V_2O_5 nanosphere compared with commercial V_2O_5. Reproduced with permission from ref. 67. Copyright 2019 Elsevier. (f) The favorable pathways of Zn^{2+} in the 3D-NRAs-V_2O_5 electrode. (g) Cycling performance for 3D-NRAs-V_2O_5 at 50 mA g^{-1} (inset: EIS spectra of different cycles). (h) Diffusion pathway of 3D-NRAs-V_2O_5 view along [100] direction. (i) The minimum energy paths for Zn^{2+} diffusion along [100] direction. Reproduced with permission from ref. 36. Copyright 2019 Elsevier.

reversibly store Zn^{2+}. However, it was only until 2016 when vanadium-based materials became the research hotspots for ZIBs cathode.

V_2O_5 has become the focus for researchers due to its unique layered structure (composed of VO_5 units in a square pyramid) and mature preparation process. However, the electron/ion transfer kinetics of V_2O_5 during the electrochemical reaction is relatively low, and the structure easily collapses during the cycle, resulting in undesirable rate performances and faster capacity decay, respectively. To alleviate that drawback, lots of strategies were employed, including nanostructuring, structural changes, cationic/molecular column supports, *etc.* It is worth noting that metal ions and water molecules inserted into interlayer of V_2O_5 could be used as "pillars" which improves structural stability and ensures the rapid electrochemical reaction kinetics.

With the different amount of metal ions incorporated into vanadium oxides layer, the formed metal vanadate exhibits different crystal structures and distinct electrochemical performances, furnishing a wide range of options for ZIBs cathode. Other than vanadium oxides and vanadates, thanks to the strong induction of the $[PO_4]$ tetrahedron, vanadium phosphate generally has a higher redox potential than those of the aforementioned, which is promising for higher energy density. In this section, the progresses and reaction mechanism of vanadium oxides, vanadates, and vanadium phosphates nanomaterials for rechargeable ZIBs are summarized and discussed in detail. **Table 1** presents the typical reported vanadium-based nanomaterials and their electrochemical properties for zinc ion batteries.

3.1. Vanadium oxides

With variety of oxidation state, vanadium oxide has several variants, including but not limited to orthorhombic V_2O_5, double-layer $V_2O_5{\cdot}nH_2O$, $V_{10}O_{24}$, $V_3O_7{\cdot}H_2O$, V_6O_{13}, VO_2, and V_2O_3. Among them, the orthorhombic V_2O_5 and double-layer $V_2O_5{\cdot}nH_2O$ exhibit a typical layered structure with the opened channel that is easy for ion insertion between interlayers. However, despite being studied for other battery systems including LIBs for decades, vanadium oxides have shown the characteristics of low voltage and poor ion storage. Recently, the research on vanadium oxide in ZIBs has attracted extensive attention.

3.1.1. V_2O_5

On account of the two-electron redox center, large interlayer spacing (up to 0.44 nm) and high theorical zinc storage capacity (589 mAh g^{-1}), bilayer vanadium pentoxide (V_2O_5) possesses enormous potentials as cathode materials for zinc ion storage.[36, 37] A broad open channel is provided by the layered structure allowing metal ions to insert or extract conveniently, which shows that the intercalation behavior is pseudo-capacitive. Many efforts have been made to figure out the reaction mechanism of zinc ion towards layered V_2O_5.[20-22, 38-40] In 2018, a rechargeable Zn-V_2O_5 energy supply system was reported by Zhang *et al.* with outstanding specific capacities and excellent stability at room temperature and extreme conditions (-10 °C and 50 °C) using 3M $Zn(CF_3SO_3)_2$ as electrolyte (**Fig. 2**a).[41] The *ex-situ* X-ray diffraction (XRD) and *ex-situ* X-ray photoelectron spectroscopy (XPS) were used to explore the mechanism of zinc storage. As revealed in Fig. 2b, during discharging, the X-ray diffraction peak of V_2O_5 gradually decreases, while other peaks emerge which can be assigned to $Zn_xV_2O_5{\cdot}H_2O$. This result indicated that the insertion of Zn^{2+} and H_2O enlarged the interlayer spacing, and the pristine layered V_2O_5 was converted into $Zn_xV_2O_5{\cdot}H_2O$. *Ex-situ* XPS indicated that during discharge, the valence state of vanadium changes to a lower value, which further proves the insertion of Zn^{2+}. During charging, the V 2p spectrum can be recovered to almost initial state, indicating the high reversibility of V_2O_5 electrode (Fig. 2c). Therefore, the V_2O_5 cathode exhibits a remarkable capacity of 372 mAh g^{-1} and the excellent cyclability of 4000 cycles with 91.1% capacity retention (Fig. 2d). Moreover, this aqueous battery demonstrates superior rate capability (Fig. 2e). An impressive reversible capacity as high as 386 mAh g^{-1} was successfully achieved at a current density of 10 A g^{-1}, accompanied with capacity retention of 83.7%. In addition, the morphology of V_2O_5 turns into a porous structure after 100 cycles during

Table 1. The typical vanadium-based nanomaterials and their electrochemical properties for zinc ion batteries.

View Article Online
DOI: 10.1039/D0QM00577K

Materials	Electrolyte	Operating voltage	Electrochemical performance				Ref.
			Current density (mA g^{-1})	Cycling number	Capability (mAh g^{-1})	Retention (%)	
NC@V_2O_5	$ZnCl_2$ in PVA	0.3-1.6 V	300	400	458	85.3	42
V_2O_5	$Zn(CF_3SO_3)_2$	0.3-1.5 V	100	100	401	/	43
			2000	1000	230	73	
TiN@ V_2O_5NWA/CNTF	2 M $ZnSO_4$·$7H_2O$	0-1.6 V	0.5	/	636	/	38
BL-V_2O_5	0.5 M AN-$Zn(TFSI)_2$	0.3-1.5 V	100	120	170	/	44
V_2O_5·$6H_2O$	3 M $Zn(CF_3SO_3)_2$	0.2-1.6 V	500	100	354.8	/	45
			2000	1000	297	94	
VO_2 (D)	3 M $ZnSO_4$	0.2-1.5 V	100	/	408	/	46
			20000	/	200	/	
			3000	1200	298	78	
VO_2 (B)	$Zn(CF_3SO_3)_2$	0.3-1.5 V	50	50	357	/	47
			58000	/	171	/	
V_3O_7·H_2O	1 M $ZnSO_4$/H_2O	0.4-1.1 V	1500	/	325	/	48
			3000	/	270	80	
	0.25 M $Zn(CF_3SO_3)_2$/AN	0.5-1.8 V	375	50	175	/	
V_3O_7·H_2O/rGO	1 M $ZnSO_4$	0.3-1.5 V	1500	1000	202	79	49
V_6O_{13}·nH_2O	3 M $Zn(CF_3SO_3)_2$	0.2–1.4 V	100	50	395	/	50
			5000	1000	262	87	
$V_{10}O_{24}$·$12H_2O$	3 M $Zn(CF_3SO_3)_2$	0.3-1.6 V	1000	300	355	/	51
			5000	3000	301	98	
V_2O_3@C	3 M $Zn(CF_3SO_3)_2$	0.3-1.5 V	100	/	350	/	52
			5000	4000	165	90	
LiV_3O_8	1 M $ZnSO_4$	0.6-1.2 V	133	65	200	75	53
$Na_{0.33}V_2O_5$	3 M $Zn(CF_3SO_3)_2$	0.2-1.6 V	100	1000	367.1	93	54
C-KVO|Od	2 M $Zn(CF_3SO_3)_2$	0.1-1.7 V	200	200	385	/	55
			20000	1000	166	95	
$Mg_xV_2O_5$·nH_2O	3 M $Zn(CF_3SO_3)_2$	0.1-1.8 V	100	200	353	/	56
			1000	1000	264	80	
$Ca_{0.2}V_2O_5$·nH_2O	1.0 M $ZnSO_4$	0.6-1.6 V	200	/	340	/	57
			80000	5000	~60	96	
$Mn_{0.15}V_2O_5$·nH_2O	1 M $Zn(ClO_4)_2$ in PC	0.2-1.7 V	0.1	/	367	/	58
			10000	8000	153	80	
			2000 (-20 °C)	3000	100	/	
$Zn_{0.25}V_2O5$·nH_2O	1M $ZnSO_4$	0.5-1.4 V	300	/	282	/	59
			2400	1000	260	81	
δ-$Ni_{0.25}V_2O_5$·nH_2O	3 M $ZnSO_4$	0.3-1.4 V	200	50	402	95	60
			5000	1200	218	98	
$Ag_2V_4O_{11}$	0.5 M $Zn(CF_3SO_3)_2$	0.4-1.7 V	200	/	213	/	61
			5000	6000	100	93	
$NH_4V_4O_{10}$	2 M $ZnSO_4$	0.4–1.4 V	10000	1000	255.5	/	62
$Na_3V_2(PO_4)_3$	0.5 M $Zn(CH_3COO)_2$	0.8-1.8 V	1000	200	108	93	63

View Article Online
DOI: 10.1039/D0QM00577K

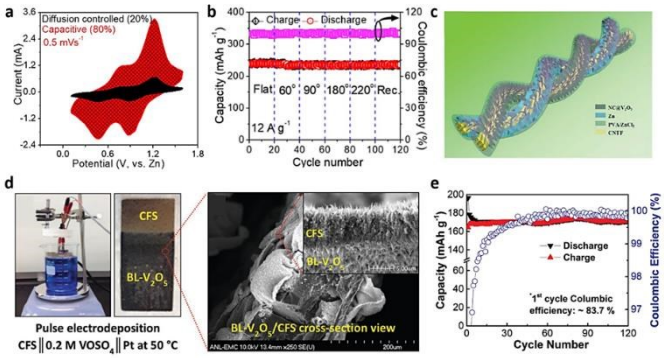

Fig. 4 (a) The capacitive contribution at 0.5 mV s^{-1} of Ti-V_2O_5 cathode. (b) The capacity profiles under various bending states at 12 A g^{-1}. Reproduced with permission from ref. 68. Copyright 2020 Elsevier. (c) Schematic illustration of the fiber-shaped CNTF@NC@V_2O_5 cathode. Reproduced with permission from ref. 42. Copyright 2019 The Royal Society of Chemistry. (d) Pictures of pulse electrodeposition for BL-V_2O_5 on CFS and the corresponding SEM image. (e) The cycling stability of BL-V_2O_5 electrode at 10 C. Reproduced with permission from ref. 44. Copyright 2016 WILEY-VCH.

repeated Zn^{2+} insertion and exaction as confirmed by post-mortem transmission electron microscopy (TEM) images (Fig. 2f) This unique porous structure could provide more active sites for Zn^{2+} storage and a low barrier energy for the Zn^{2+} intercalation/deintercalation processes, resulting in an increase of initial capacity and excellent rate capability of V_2O_5 electrode. The reaction mechanism can be summed up in this equation:

$$V_2O_5 + x\ Zn^{2+} + 2\ x\ e^- + n\ H_2O \leftrightarrow Zn_xV_2O_5{\cdot}nH_2O \quad [1]$$

While great successes were achieved, most V_2O_5 cathode still suffers from certain difficulties such as low ion diffusion, low conductivity, dissolution of materials, and self-aggregation. To further overcome these drawbacks, it is reported that the intercalation of H_2O molecules into V_2O_5 interlayer could efficiently enlarge the interlayer spacing, offering a rapid zinc ion transport pathway.[44, 64] To further enhance the electrochemical performances, recent studies have found that the vanadium oxides with mixed-valence could also enhance the charge transfer kinetics by increasing the electrical conductivity and ionic conductivity via electron hopping between V^{4+} and V^{5+} ions and forming the extra oxygen vacancy, respectively.[65] Specifically, a simple *in-situ* method was developed by Zhao *et al*. to introduce V^{4+} and V^{5+} at the same time, increasing the amount of interlayer water while expanding the distance between layers to avoid the import of exogenous cations together with the dehydration of V_2O_5 nanosheets.[66] As revealed by scanning electron microscopy (SEM) (**Fig. 3**a), the layer-expanded $V_2O_5{\cdot}2.2H_2O$ (E-VO) electrode exhibits a typical three-dimensional porous architecture composed of interconnected ultrathin nanoflakes with large lateral size. The high-resolution transmission electron microscopy (HRTEM) image indicates high exposure of [001] facets, allowing the preparation of flexible binder-free electrode. According to X-ray absorption near edge structure (XANES) spectra, the K-edge of E-VO cathode locates between V_2O_5 and VO_2 standard spectra, revealing that V in E-VO is of mixed-valence (Fig. 3b). The author claimed that the appearance of mixed-valence in E-VO is beneficial to the conductivity. In addition, the generation of oxygen vacancy can still maintain electroneutrality, which could effectively improve the ion transfer rate while ensuring the structure stability of electrode materials. In conclusion, the improvement of zinc storage performance compared to standard V_2O_5 is ascribed to the formation of mixed-valence, the increase of the amount of interlayer water and the expansion of layer spacing (Fig. 3c).

The development of well-defined electrode structures is of great importance in improving electrochemical performance.[21, 36, 43, 67] For instance, hollow structures could effectively alleviate volume expansion during charge-discharge. Chen *et al.* reported a hollow V_2O_5 nanospheres fabricated by the template-free solvothermal approach.[67] The SEM image shows that the as-prepared V_2O_5 particles exhibit hollow structure with high uniformity (Fig. 3d). As can be seen in Fig. 3e, when employed as cathode materials for ZIBs, this hollow nanospheres display outstanding rate capability performance. In another example, Chen *et al*. reported the viability of V_2O_5 nanorods constructed 3D porous architectures (3D-NRAS-V_2O_5) architecture as cathode.[36] As presented by SEM image, the individual cluster of porous 3D-NRAS-V_2O_5 is constituted of major amount of nanorods interweaving tightly each other (Fig. 3f). This structure composed of nanosized building blocks has the combined benefits of increased interaction with the electrolyte and decreased load/mass diffusion pathways. As a result, a remarkable capacity of 336 mAh g^{-1} at 50 mA g^{-1} was delivered (Fig. 3g). Apparent capacity increase in the first 50 cycles can be attributed to the activation process. On the basis of the first-principle calculation, the author emphasized that the pathway along the [100] channel is of most feasibility for Zn^{2+} intercalation into the interlayer of V_2O_5, which exhibits energy barrier as low as 0.69 eV (Fig. 3h and Fig. 3i).

Direct growth of nanostructured active materials on flexible conductive substrates is one of the most effective way to improve electrode kinetic and while giving flexibility aspect to the ZIB. The most commonly used substrates include carbon clothes (CC), carbon nanotubes (CNTs), graphene-based materials, nickel foam, titanium, and so forth.[19, 22, 45, 68, 69] Gaved *et al.* reported a binder-free cathode for ZIBs consisting of ultrathin 2D V_2O_5 nanosheets on titanium substrate.[68] Owing to the merits of numerous exposed active sites, enlarged electrode-electrolyte contact, accelerated charge transfer, and facilitated mass diffusion, this two-dimensional flexible Ti-V_2O_5 cathode has a good command of rapid insertion/extraction of zinc ions, bringing out a higher pseudo-capacitive storage of up to 80% at 0.5 mV s^{-1} (**Fig. 4**a). Due to the high flexibility of the Ti-V_2O_5 cathode, the assembled Zn//Ti-V_2O_5 system manifests excellent electrochemical performance and energy characteristics under different bending states (Fig. 4b). Similarly, He *et al.* fabricated a hierarchical core-shell nanostructure using V_2O_5 deposited on carbon nanotube fibers (CNTF), which significantly enhanced the charge transfer and mass diffusion of the cathode (Fig. 4c).[42] Besides, benefitting from the unique 3D structure, the binder-free CNTF@NC@V_2O_5 cathode delivered

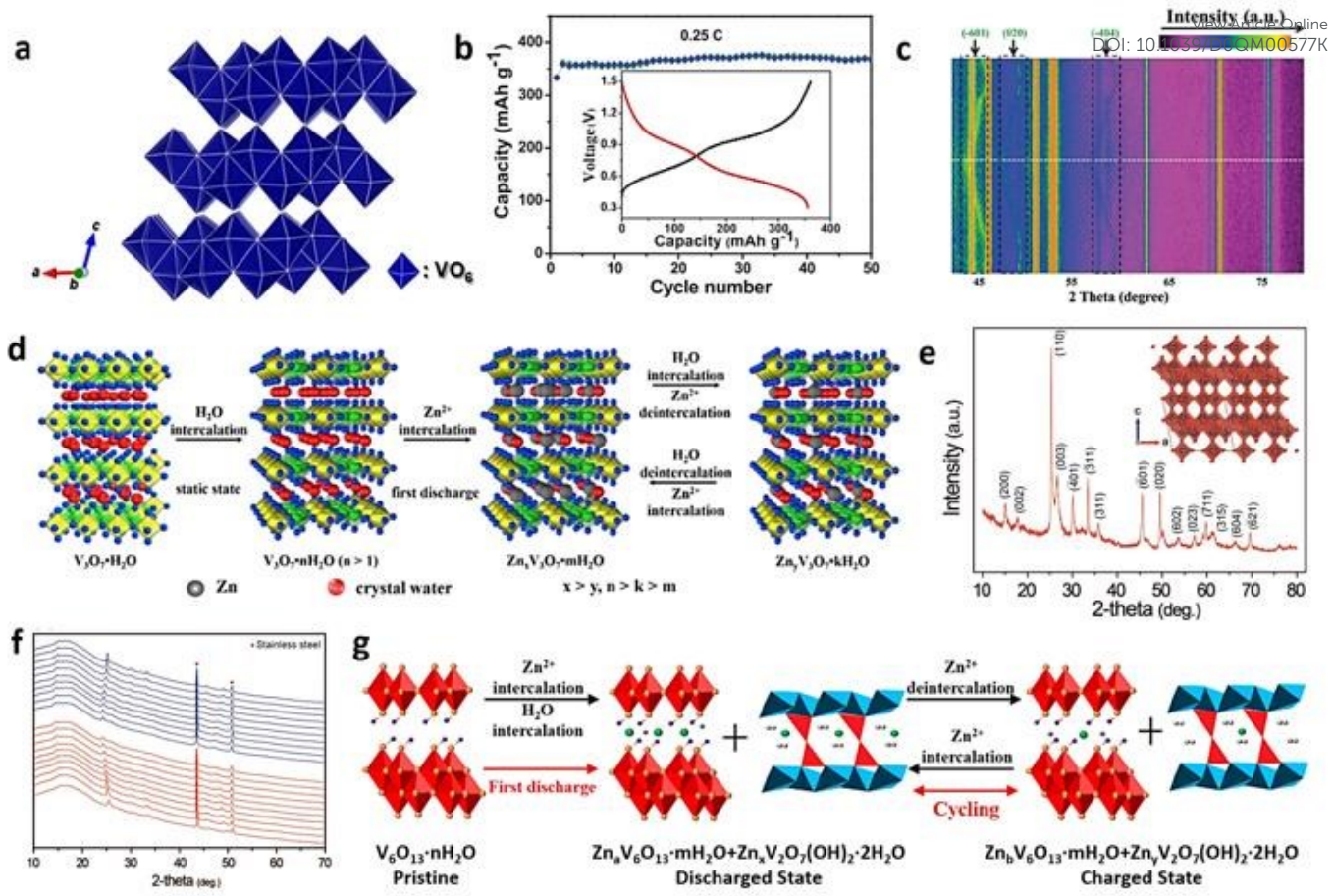

Fig. 5 (a) The crystal structure of VO_2(B). Reprinted with permission from ref. 77. Copyright 2018 American Chemical Society. (b) The cycling stability of VO_2(B) at 0.25 C. (c) In-situ XRD peak intensities of VO_2(B) nanowires. Reproduced with permission from ref. 47. Copyright 2018 WILEY-VCH. (d) Reaction mechanism of the Zn/rGo-V_3O_7 system. Reproduced with permission from ref. 49. Copyright 2018 American Chemical Society. (e) XRD pattern of pristine V_6O_{13} powder (inset: the crystal structure along [010]). (f) Ex-situ XRD results of V_6O_{13}. Reproduced with permission from ref. 83. Copyright 2019 WILEY-VCH. (g) The reaction mechanism during Zn^{2+} insertion/extraction of V_6O_{13}. Reprinted with permission from ref. 50. Copyright 2019 American Chemical Society.

an outstanding capacity retention of 85.3% after 400 cycles. Moreover, the fiber-shaped battery could achieve the volumetric energy density of 85.8 mWh cm^{-3} and a power density of 5.6 W cm^{-3}, higher than those of most reported aqueous energy storage devices. Li *et al*. also reported a binder-free cathode for fiber-based zinc ion battery, which also used CNTF as the substrate. Benefiting from the synergistic effect of highly conductive TiN nanowire arrays (NWAs) and layered V_2O_5 nanosheets, the TiN@V_2O_5 NWAs/CNTF cathode revealed the excellent zinc ion storage performances. These fiber-based zinc ion batteries satisfy with the desire for high energy density in low-volume energy-storage devices.

In addition to the aqueous ZIBs system, the hydrated V_2O_5 in the non-aqueous ZIBs system was also studied. One advantage of the non-aqueous ZIBs system is that it is not limited by the water decomposition voltage, therefore, nonaqueous ZIBs could achieve the goal of high voltage and power density. Zn//V_2O_5 battery with a nonaqueous acetonitrile-zinc(II) bis (trifluoromethanesulfonyl) imide ((AN)-Zn$(TFSI)_2$) electrolyte was investigated by Senguttuvan *et al*.[44] The V_2O_5 was directly grown on carbon foams substrate (CFS) via electrodeposition technique, which was expected to percolate the electrons effectively during redox reactions (Fig. 4d). The electrochemical properties in Zn^{2+} storage of V_2O_5/CFS are shown in Fig. 4e. Noteworthy, it was found that the coulombic efficiency is close to 100%. It should be pointed out that, in the aqueous ZIBs system, the Zn^{2+} participating in the reaction are hydrated, not the insertion/extraction of pure zinc ions. Nevertheless, in the first hydration layer, the exact amount of water molecules still remains a mystery. The majority of investigators believed that the hydrated Zn^{2+} ions are more suitable for insertion into the host materials due to their reduced electrostatic interaction, which explains the higher coulombic efficiencies of aqueous system compared to that of nonaqueous system.

3.1.2 VO_2

Among over ten phases of VO_2,[70] the metastable VO_2(B) is the most stable and possesses outstanding energy storage performances towards. VO_2(B) is constructed from VO_6 octahedron (**Fig. 5**a), which shares angles and edges to form a tunnel-like skeleton (0.82 nm^2 along *b* axis, 0.34 nm^2 along *a* axis, and 0.5 nm^2 along *c* axis). Such a big tunnel is of great convenience for the insertion of metal ions (Li^+, Na^+, and Zn^{2+} *et al*.).[71, 72] The performance of VO_2(B) as ZIBs cathode was

View Article Online
DOI: 10.1039/D0QM00577K

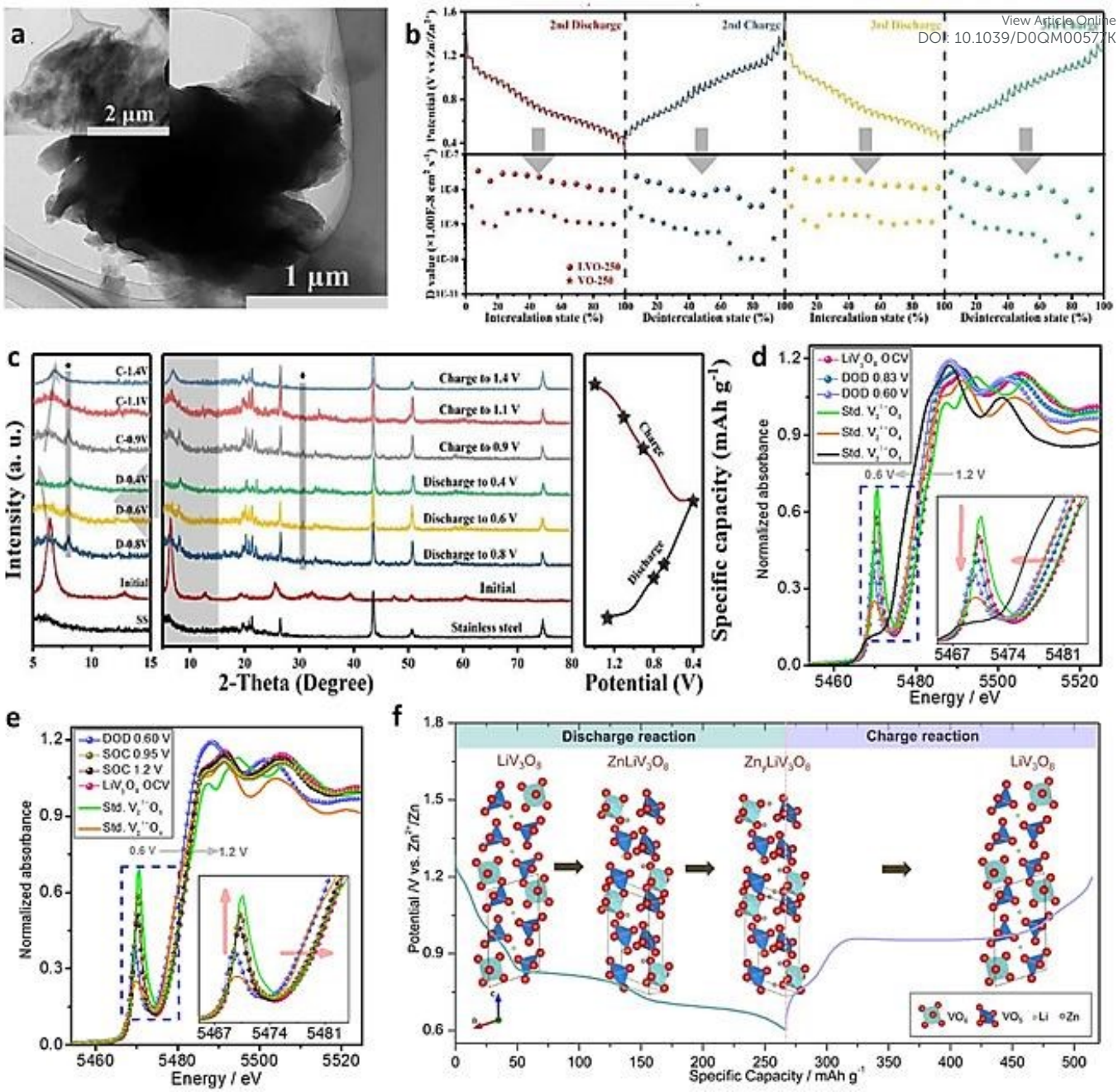

Fig. 6 (a) TEM and HRTEM images of LVO-250. (b) The discharge/charge profiles of LVO-250 measured at GITT condition and corresponding D_{Zn2+} values of LVO-250 and control samples during the 2nd and 3rd cycles. (c) Ex-situ XRD results during different voltage of LVO-250. Reproduced with permission from ref. 89. Copyright 2016 The Royal Society of Chemistry. (d, e) Comparison of normalized V K-edge XANES spectra between LVO and the standard vanadium oxides. (f) The reaction mechanism of LiV_3O_8 cathode materials. Reproduced with permission from ref. 53. Copyright 2017 American Chemical Society.

investigated by Ding *et al*. in 2018.[47] Remarkable specific capacity of 357 mAh g^{-1} at 0.25 C and an outstanding energy density of approximately 297 Ah kg^{-1} were achieved (Fig. 5b). The unique tunnel pathways delivered by VO_2(B) nanofibers facilitates the transportation of Zn^{2+} and limits the volume expansion during the insertion. *In-situ* measurement was conducted to explore the structural stability of VO_2(B) upon charging/discharging process. As revealed by Fig. 5c, three diffraction peaks located at 45.1°, 59.1°, and 49.2° assigned to (-601), (-404), and (020) were shifted to lower angles when discharging, suggesting the Zn^{2+} were gradually intercalated into the tunnels parallel to the *b* and *c*-axis. During charge, these peaks were shifted reversibly to the initial position, revealing an excellent structural stability of VO_2(B). Similarly, the VO_2(B) nanorods were fabricated by Li *et al.* through simple hydrothermal reaction and employed as cathode material for ZIBs.[73] The VO_2(B) nanorods shows outstanding cyclability and capacity within an operating voltage between 0.2 and 1.3 V. Many reported works showed that both the zinc hydroxide sulfate and H^+ are involved in the electrochemical process when

aqueous $ZnSO_4$ is used as an electrolyte.[35, 74, 75] In this work, the authors claimed that the minimal structural changes due to H^+ insertion into VO_2 were expected, which extended the cycle life. The dynamics of discharge were first started by the deposition of $Zn_4(OH)_6SO_4{\cdot}5H_2O$ and later by the injection of protons into the VO_2, both are due to the excellent rate of discharge reactions. There is a competition between the insertion of H^+ and Zn^{2+}, which is determined by the stability of the deposited compound and the energy change of H^+/Zn^{2+} in the host of vanadium oxide.[70, 71, 76-78]

Apart from VO_2(B), VO_2(A) and VO_2(D) have also been investigated as ZIBs cathode. For instance, VO_2(A) hollow spheres with outstanding electrochemical performances were synthesized by Li *et al*.[79] *Ex-situ* XRD indicated the stability of the structure with no significant shift of any diffraction peaks after charge/discharge. Moreover, monoclinic VO_2(D) hollow nanospheres with homogeneous distribution of elements were fabricated as aqueous ZIBs cathode.[46] Benefiting from the unique structure and the interior hollow architecture, excellent stability and rate performances were achieved in 3 M $ZnSO_4$.

3.1.3. $V_3O_7{\cdot}H_2O$

$V_3O_7{\cdot}H_2O$ ($H_2V_3O_8$), a mixed-valence vanadium oxide (V^{5+}/V^{4+} of 2:1), is composed of V_3O_8 layers along *a* axis that connected together by hydrogen bonds.[80, 81] The VO_6 octahedron and the VO_5 triangular bipyramid share sides and angles parallel to the *b* axis and further constitute all building blocks of $H_2V_3O_8$. The layered structure of $H_2V_3O_8$ provides spaces for the insertion of ions, while the mixed valence state implies better electrochemical performance than other single-valence vanadium oxides.[82] Recently, Kundu *et al.* reported a layered $V_3O_7{\cdot}H_2O$ for ZIBs cathode in aqueous and nonaqueous electrolyte to shed light into interfacial (de)solvation kinetics.[59] The layered $V_3O_7{\cdot}H_2O$ in aqueous electrolyte could store more than two Zn^{2+} per building block and exhibit excellent specific capacity; while performing poorly in a nonaqueous electrolyte. The operando XRD analysis showed similar structural transformation in both aqueous and nonaqueous system. The structural energetics and solid-state diffusion characteristics of Zn^{2+} are not the main factors leading to different electrochemical properties in the two media. The corresponding charge transfer resistance and activation energy in the aqueous system were reduced significantly. As a result, $V_3O_7{\cdot}H_2O$ cathode demonstrated excellent reversible zinc storage properties (375 mAh g^{-1} at 1C) in the aqueous ($ZnSO_4/H_2O$) electrolyte mainly determined by solid-state diffusion and interfacial charge transfer processes. In order to enhance the electrochemical performances of $V_3O_7{\cdot}H_2O$, Wei's group fabricated a $V_3O_7{\cdot}H_2O$/rGO cathode and a Zn/rGO anode in an aqueous ZIB system in which rGO could restrain the dendrite problem.[49] The $V_3O_7{\cdot}H_2O$ cathode delivered a remarkable specific capacity while rGO could enhance the rate capability. A splendid cyclability for 1000 cycles with capacity retention of 79% at 5 C was delivered. Fig. 5d illustrates the reaction mechanism of Zn//$V_3O_7{\cdot}H_2O$/rGO system. Due to the enhanced electrostatic attraction, water molecules are inserted into layers leading to the decrease of layer spacing, resulting in the distinctions in XRD patterns from initial state.

3.1.4. V_6O_{13}

V_6O_{13} in mixed-valence state (V^{5+} and V^{4+}) delivers high electron conductivity at room temperature, which is conducive to ultra-fast reaction process. The crystalline structure of V_6O_{13} is comprised of VO_6 octahedrons with shared corners and edge distortions. They are connected to each other through shared corners to form single or double vanadium oxide layers. In the double layer, only small part of V sites exhibits the property of V^{5+} while the remaining V sites are occupied by V^{4+}. In 2019, Shin *et al.* reported a V_6O_{13} with high crystallinity (Fig. 5e), projected down to the *b* axis.[83] When applied to ZIBs cathode between 0.2 and 1.6 V, it could deliver a prolonged cyclability for 2000 cycles. *Ex-situ* XRD were used to study the intercalation behavior of Zn^{2+} (Fig. 5f). In these XRD diffractograms, the overall trend of diffraction peak shifts is consistent, *i.e.* while the peak position during discharge shift to lower angles (increase of d-spacing), the reverse is seen during charge (decrease of d-spacing). Moreover, benefiting from the preponderance of stable architecture as well as the expanded interlayer spacing, Lai *et al*. synthesized a $V_6O_{13}{\cdot}nH_2O$ hollow micro flower consisting of ultrathin nanoflakes, which showed a remarkable capacity and good cyclability performance.[50] Very recently, an oxygen-deficient V_6O_{13} cathode with alternating single and double vanadium oxide layers was fabricated by Peng *et al.* in 2020, which was enriched with oxygen vacancies to create more divalent cation-intercalating sites and there by enhance capacity.[84] The Zn^{2+} storage mechanism for $V_6O_{13}{\cdot}nH_2O$ can be reflected in Fig. 5g, and the corresponding electrochemical mechanism of cathode can be displayed as follows:

$V_6O_{13}{\cdot}nH_2O + (a+x)\ Zn^{2+} + 2\ (a+x)\ e^- + (m-n+2)$
$H_2O \leftrightarrow Zn_aV_6O_{13}{\cdot}mH_2O + Zn_xV_2O_7(OH)_2{\cdot}2H_2O$ (the first charge process) [2]

$Zn_aV_6O_{13}{\cdot}mH_2O + Zn_xV_2O_7(OH)_2{\cdot}2H_2O \leftrightarrow$
$Zn_bV_6O_{13}{\cdot}mH_2O + n\ x\ V_2O_7(OH)_2{\cdot}2H_2O +$
$(a+x-b-y)\ Zn^{2+} + 2\ (a+x-b-y)\ e^-$ (subsequent cycles) [3]

3.1.5. $V_{10}O_{24}{\cdot}12H_2O$

$V_{10}O_{24}{\cdot}12H_2O$ can be considered as an oxygen-deficient $V_2O_5{\cdot}nH_2O$ or as a representative hydrated vanadium oxide with mixed-valence (V^{5+}/V^{4+} ratio is 4:1).[85] A layered $V_{10}O_{24}{\cdot}12H_2O$ (VOH) with large interlayer spacing (1.4 nm) and high valence state (4.8) was fabricated through a facile hydrothermal method by Liu *et al.*[86] Owing to partially reduction V_2O_5, the reduction of particle size, and the stability of interlayer water molecules, the VOH cathode showed a stable cyclability (115 mAh g^{-1} at 1 A g^{-1} for 3000 cycles). To enhance its electrochemical performance, elemental doping is usually employed. Li *et al.* developed a layered $V_{10}O_{24}{\cdot}12H_2O$ as cathode for aqueous ZIBs, which delivered an excellent cyclability for 3000 cycles after Al doping.[51] The Al doped $V_{10}O_{24}{\cdot}12H_2O$ shows an urchin-like morphology consisting of thinner belts. Benefiting from the unique layer structure, Al doped $V_{10}O_{24}{\cdot}12H_2O$ cathode showing an outstanding cyclability with 98% capacity retention after 3000 cycles, which is superior to 65% in the pure $V_{10}O_{24}{\cdot}12H_2O$. The significant improvement

in long-term cycling performance indicates that aluminum doping is an alternative opportunity to further develop revolutionary vanadium oxides materials in ZIBs. The reaction of the Zn//$V_{10}O_{24}$·12H_2O system can be described using the following equation:

$$V_{10}O_{24}\cdot 12H_2O + x\ Zn(H_2O)_m^{2+} + 2\ x\ e^- \leftrightarrow Zn_xV_{10}O_{24}\cdot nH_2O \quad [4]$$

3.1.6. V_2O_3

Vanadium sesquioxides (V_2O_3) processes typical corundum-type structures. Restricted by the special rhombohedral structure, V_2O_3 could hardly provide sufficient sites for Zn^{2+} insertion, which fails to be effectively discharged as a cathode material in ZIB. Nevertheless, if the reversible two-electron redox of V_2O_3 is fully realized, a high capacity can be reached up to 715 mAh g^{-1} by taking the advantage of its high conductivity. Surprisingly, through an *in-situ* anodic oxidation strategy, Dou *et al.* reported a V_2O_3 cathode with high performance.[87] Efficient anodic oxidation process of V_2O_3 cathode was achieved during the first charging process by simultaneously regulating the concentration of the electrolyte and the morphology of V_2O_3. Moreover, what noteworthy is that owing to the low valence state of vanadium (V^{3+}), V_2O_3 tends to be easily oxidized. To solve this problem, carbon coating may be a practical method to improve the stability in air. Therefore, a porous V_2O_3@C cathode was fabricated for aqueous ZIBs by Ding *et al*.[52] The unique channel and the proper pore size distribution of V_2O_3 are favorable for penetration of zinc ions, offering a good rate performance. The electrochemical reaction for V_2O_3 cathode can therefore be illustrated as the following equations:

$$V_2O_3 + x\ Zn^{2+} + n\ H_2O + 2\ x\ e^- \leftrightarrow Zn_xV_2O_3\cdot nH_2O \quad [5]$$

3.2. Vanadates

The deformability of vanadium-oxygen polyhedron and the change of vanadium valence state cause the vanadium oxides structure to have a strong adaptability to compound with other cations; thus, generating a large number of derivatives with various M-V-O structures (M stands for metal ions or NH_4^+), which are called as vanadates. Many works related to vanadates have been reported so far, most of which are in Li^+ storage research, with different compositions, structure and properties. Generally, the introduction of cations will yield some benefits and lead to splendid electrochemical properties. A lot of reported alkali vanadates (such as $Na_{0.33}V_2O_5$ and $K_{0.25}V_2O_5$) illustrate a better cycling stability than pure V_2O_5 when used as cathodes in lithium batteries owing to their "pillar" effect of the alkali metal ions. The composed vanadates have shown numerous different crystal structures with various electromagnetic characteristics through the addition of different metal ions, offering a wide range of options to research new metal-ion batteries.

3.2.1. Alkali vanadates

Most of the vanadates usually show more attractive electrochemical performances compared to the pristine vanadium oxides. In this part, we introduce alkali vanadate in three categories, namely, lithium vanadates, sodium vanadates, and potassium vanadates. The addition of alkali metal ions has great effects on the structure and electrochemical properties. For example, K^+ ions in $K_2V_6O_{16}$·2.7H_2O act as "pillars" to bring a

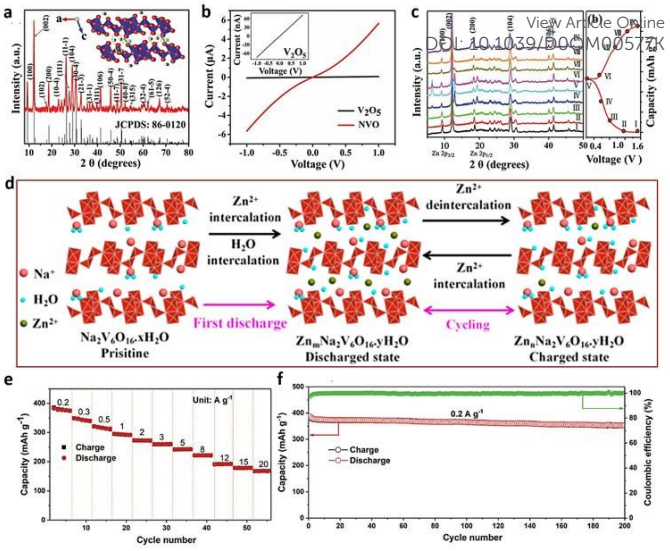

Fig. 7 (a) The XRD pattern together with the corresponding crystal structure of $Na_{0.33}V_2O_5$. (b) The *I-V* profiles of NVO and control sample. (c) The ex-situ XRD results of NVO electrode at different voltage states. Reproduced with permission from ref. 54. Copyright 2018 WILEY-VCH. (d) Schematic illustrations of $Na_2V_6O_{16}$ during charging and discharging processes. Reprinted with permission from ref. 94. Copyright 2018 American Chemical Society. (e, f) Rate performances and cycling stability of C-KVO|Od electrode. Reproduced with permission from ref. 55. Copyright 2019 WILEY-VCH.

stabilizing effect. It effectively improves the structural stability and the size of ion diffusion channel; thereby, enhancing the cyclability and rate capability as compared to V_2O_5.[88] Alkali metal vanadates have been used for Li and Na storage system for decades; however, applications of alkali metal vanadate for ZIBs is only emerged while in recent years.

Yang *et al.* reported an cotton-like lithium vanadate (LVO-250) electrode as Zinc ion cathode with an enlarged layer spacing of 13.77 Å in (001) face compared to VO-250 (12.0 Å in (001) face), which effectively facilitates Zn^{2+} diffusion (**Fig. 6**a).[89] Therefore, the LVO-250 shows an outstanding rate performance and cyclability under extreme condition (0-50 °C), revealing the excellent temperature adaptability in practical application. At room temperature, LVO-250 electrode displays a reversible capacity of 232 mAh g^{-1} at 5 A g^{-1} with a remarkable cyclability. The Galvanostatic Intermittent Titration Technique (GITT) tests reflect a higher diffusion coefficient (D_c) compared to control samples (Fig. 6b). As revealed in Fig. 6c, the *ex-situ* XRD were performed to analyze Zn^{2+} storage mechanism of LVO-250 electrode. When discharging, the diffraction peak located at 6.2° that corresponding to the (001) plane shifted to a lower angle, which recovered to the initial state during charging process. This phenomenon can be attributed to the fact that Zn^{2+} ions are inserted into the layers of LVO-250 during the discharge, resulting in the expansion of the interlayer space. Moreover, two other phases of $Zn_{0.25}V_2O_5$·nH_2O and $Zn_{0.29}V_2O_5$ appeared and gradually increased during charging, reflecting the process of Zn^{2+} intercalation into layered LVO-250 electrode. To further explore the working principle of lithium vanadate, Alfaruqi *et al.*

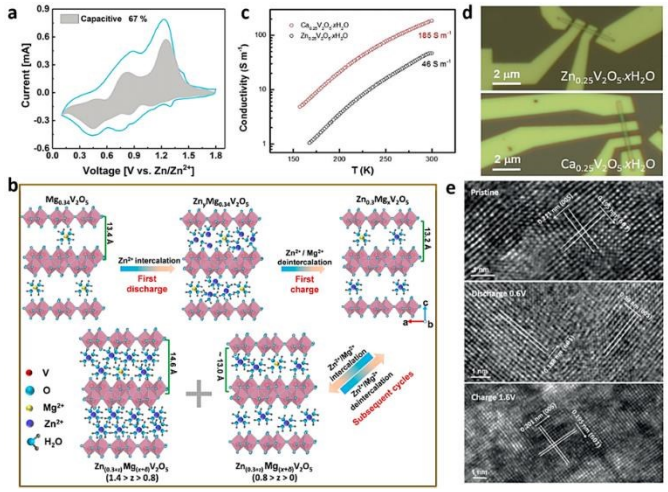

Fig. 8 (a) The capacitive contribution of $Mg_{0.34}V_2O_5$ at 0.3 mV s^{-1}. (b) Reaction mechanism illustration of $Mg_{0.34}V_2O_5$ for Zn^{2+} storage. Reproduced with permission from ref. 56. Copyright 2018 American Chemical Society. (c, d) The individual CVO and $Zn_{0.25}V_2O_5{\cdot}nH_2O$ based nanodevices, and their electricity conductivities. (e) HRTEM images of CVO electrode at various voltage states. Reprinted with permission from ref. 57. Copyright 2018 Wiley-VCH.

prepared a layered LiV_3O_8 (LVO), as an intercalated cathode of ZIBs with high storage capacity.[53] *Ex-situ* XANES analyses were carried out to probe the change in vanadium oxidation states after Zn^{2+} insertion/extraction process (Fig. 6d and Fig. 6e). The main edge features before electrochemical process are identified as the standard V^{5+} in pure vanadium pentoxide. Remarkably, during continuous charging, the main absorption peak moves gradually toward the high energy direction (or positive displacement), indicating the increase in valence states of vanadium. The schematic illustration of the reaction mechanism is shown in Fig. 6f.

Sodium vanadate (NVO) is the most reported ZIBs cathode material in the family of alkali metal vanadate .[90-93] With larger diameter of Na^+ compared to that of Li^+ , the interlayer spacing of is larger than that of lithium vanadate. This makes sodium vanadate more conducive to the insertion and extraction of Zn^{2+}. Three different vanadium sites can be founded in the crystal structure of NVO, which could be abbreviated as V(a), V(b) and V(c). $V(a)O_6$ octahedron forms a zigzag chain, while $V(b)O_6$ octahedron forms a double chain that along the direction of *b* axis. With Na^+ intercalated into the layers, $[V_4O_{12}]_n$ layer structure with $V(a)O_6$ and $V(b)O_6$ units are built by oxygen atoms along the (001) plane. The layered $[V_4O_{12}]_n$ is linked with $V(c)O_5$ and oxygen atoms at the edge to form a three-dimensional tunnel structure.[54] He *et al.* was the first to construct $Na_{0.33}V_2O_5$ (NVO) as cathode for aqueous ZIBs (**Fig. 7**a). Thanks to the stable layered structure and high electronic conductivity (5.9×10^4 S m^{-1}), the high reversible capacity as well as an exceptional cyclability were achieved (Fig. 7b). The *ex-situ* XRD shows a invertible phase transition processes between $Na_{0.33}V_2O_5$ and new phase of $Zn_xNa_{0.33}V_2O_5$ ($0 < x < 0.96$) during charge and discharge, reasoning the cycling stability of the electrode material. (Fig. 7c). The inductively coupled plasma optical emission spectroscopy analysis (ICP-OES) after cycles shows only little dissolution products (<1%) of the active material in the electrolyte, further confirming the stability of NVO during insertion and extraction of zinc ions. In 2018, Hu's group reported a $Na_2V_6O_{16}{\cdot}1.63H_2O$ (H-NVO) single-nanowire with as the cathode for ZIBs, illustrating that the H-NVO could provide an ultra-stable structure for reversible Zn^{2+} intercalation/deintercalation (Fig. 7d).[94] Moreover, if the host materials could achieve simultaneous proton and Zn^{2+} insertion/extraction, the synergistic effect between thermodynamics and kinetics of ion insertion can also be significantly enhanced. To achieve this goal, Wan *et al.* fabricated a $NaV_3O_8{\cdot}1.5H_2O$ (NVO) nanobelt composed of V_3O_8 layers and inserted Na^+, realizing the coinstantaneous insertion/extraction process of H^+ and Zn^{2+} between the V_3O_8 layers.[95] Thereby, on account of the pillars function of interlayer water and sodium ions stabilizing the V_3O_8 structure, the cathode exhibits an outstanding capacity as well as an enhanced cyclability of 1000 cycles. The authors claimed that the outstanding electrochemical properties could also be attributed to Na^+ addition into $ZnSO_4$ electrolyte, which inhibits the dissolution of the active materials and Zn dendrite deposition synchronously. Below are electrochemical reactions formulas of the Zn/NVO aqueous batteries:

First discharge:

$$NaV_3O_8{\cdot}1.5H_2O + 0.65\ ZnSO_4 + 6.5\ H_2O + 2.45\ Zn \leftrightarrow 0.65\ Zn_4SO_4(OH)_6{\cdot}4H_2O + H_{3.9}NaZn_{0.5}V_3O_8{\cdot}1.5H_2O \quad [6]$$

Subsequent cycles:

$$0.65\ Zn_4SO_4(OH)_6{\cdot}4H_2O + H_{3.9}NaZn_{0.5}V_3O_8{\cdot}1.5H_2O \leftrightarrow NaZn_{0.1}V_3O_8{\cdot}1.5H_2O + 0.65\ ZnSO_4 + 6.5\ H_2O + 2.35\ Zn \quad [7]$$

Potassium vanadate as ZIBs cathode materials could also provide outstanding electrochemical performance.[88, 96] A unique 3D structure of C-KVO|O_d with oxygen defect and carbon engineering was studied by Yang *et al.*[55] As shown in Fig. 7e and Fig. 7f, by virtue of the enhanced electrical conductivity of carbon hybrids and promoted diffusion/adsorption of reactants, this cathode presented an outstanding specific capacity and remarkable rate-capability performance. More importantly, the existence of oxygen vacancies in C-KVO|O_d lattice significantly decreases the Gibbs free energy (-0.22 eV) of Zn^{2+} adsorption, which is 1.33 eV lower than that of KVO, indicating that the adsorption/desorption of Zn^{2+} in oxygen defective KVO is highly reversible. Moreover, the carbon-coated porous structure can facilitate the charge transfer and furnish more active site for Zn^{2+} storage. The synergistic effect of these two factors endows the rapid insertion/extraction of Zn^{2+} into C-KVO|O_d host.

3.2.2. Alkali earth vanadates

Alkaline earth metal vanadate was long overlooked as electrode materials for energy storage applications as opposed to alkaline earth metal vanadate. However, recent studies of alkaline earth metal vanadates have shown that the electrochemical performance in this field really deserves more attention. Alkali earth vanadate usually exhibits layered structure, with inserted metal ion (e.g., Be, Mg, Ca) and water as "pillars" to guarantee the structure stability. Recent studies

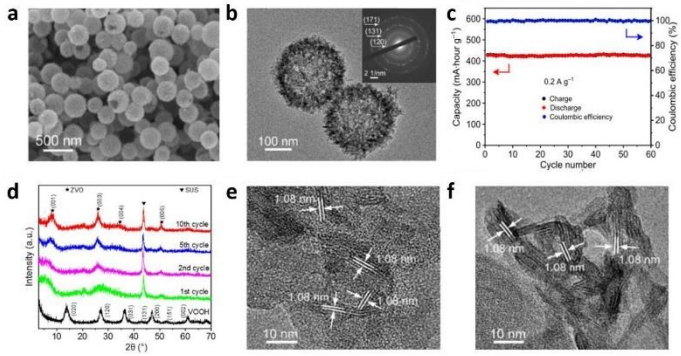

Fig. 9 (a) SEM image of VOOH nanospheres. (b) TEM and SAED images of ZVO nanoflower. (c) Cycling stability of ZVO electrode at 0.2 A g^{-1}. (d) XRD patterns of VOOH electrode at different cycling stages. (e, f) Ex-situ HRTEM images of the ZVO electrode at fully charged and discharged states. Reproduced with permission from ref. 104. Copyright 2019 American Association for the Advancement of Science.

revealed that alkali earth vanadate could provide superior electrochemical performance toward Zn^{2+} storage.[97, 98] For instance, the Mg-intercalated V_2O_5 possesses high energy density and theoretical capacity for Zn ion cathode than ZVO owing to the smaller molecular weight of Mg^{2+}. Ming *et al.* reported a $Mg_{0.34}V_2O_5{\cdot}nH_2O$ (MVO) nanobelts with a porous structure at a wide voltage window between 0.1 and 1.8 V versus Zn^{2+}/Zn (**Fig. 8**a).[56] With the expanded interlayer spacing of 1.34 nm, excellent specific capacity and outstanding rate performance have realized in this system. By the analysis of *ex-situ* XRD, Raman, TEM, and XPS, the reaction mechanism during electrochemical charge and discharge processes of MVO can be illustrated as Fig. 8b. The electrode reaction can be summarized as follows:

$$Zn_{0.3}Mg_xV_2O_5 + z\,Zn \leftrightarrow Zn_{(x+0.3)}Mg_xV_2O_5 \quad [8]$$

Surprisingly, as the content of Zn^{2+} increases, the inserted Zn^{2+} combined with water molecules could reduce the electrostatic repulsion between layers. Moreover, the formation of hydrogen bonds among Zn^{2+} and H_2O further narrowing the layer spacing. These two factors induce the decrease of interlayer spacing, making the XRD diffraction peaks shift to the higher angles.

A $Ca_{0.25}V_2O_5{\cdot}nH_2O$ nanobelt was also reported by Xia *et al.* for the application in Zn ion storage.[57] With the higher electrical conductivity (185 S m^{-1}) than that of $Zn_{0.25}V_2O_5{\cdot}nH_2O$ (46 S m^{-1}), the impressive cycling performance was obtained (Fig. 8c and Fig. 8d). During discharge, the author suggested that the intercalation of Zn^{2+} can bring out a contraction of interlayer spacing because the intercalated Zn^{2+} attracts the adjacent cations; consequently, the crystal structure can be recovered by reversing the voltage, as shown by the HRTEM images in Fig. 8e. This finding is parallel to the $Mg_{0.34}V_2O_5{\cdot}nH_2O$ which we have mentioned before. The similar reaction mechanism also can be seen in the case of $CaV_6O_{16}{\cdot}3H_2O$ and $BaV_6O_{16}{\cdot}3H_2O$ cathodes, which demonstrate excellent reversibility of Zn^{2+} (de)intercalation.[97, 99]

3.2.3. Transition metal vanadates

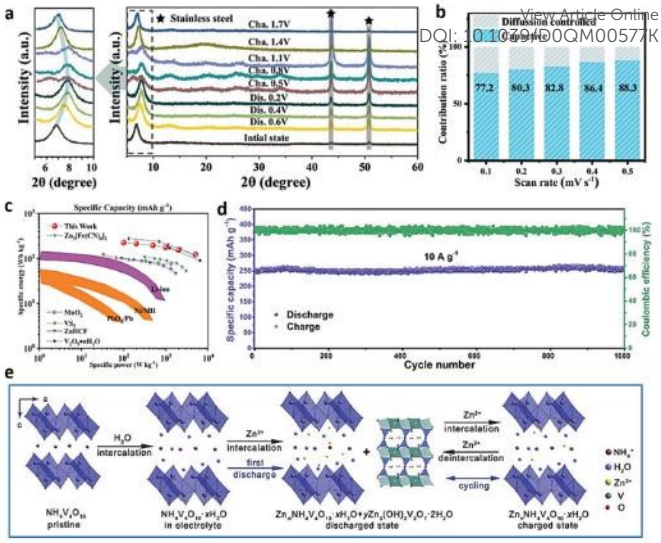

Fig. 10 (a) The ex-situ XRD patterns at various voltage state of MnVO electrode. Reproduced with permission from ref. 58. Copyright 2019 WILEY-VCH. (b) Normalized contribution ratio of capacitive and diffusion-controlled capacities of AVO electrode. Reproduced with permission from ref. 61. Copyright 2019 WILEY-VCH. (c) Ragone plots of energy density versus power density compared with other standard devices. Reproduced with permission from ref. 112. Copyright 2018 The Royal Society of Chemistry. (d) Cycling stability for $NH_4V_4O_{10}$ at 10 A g^{-1}. (e) Reaction mechanism illustration of $NH_4V_4O_{10}$ showing the intercalation intercalation/extraction for H_2O and Zn^{2+}. Reproduced with permission from ref. 62. Copyright 2019 The Royal Society of Chemistry.

With various compositions, structures and properties, transition metal vanadates have a large number of family members. To tackle the limitations such as poor rate performances, unsatisfied cyclability, and limited specific capacity, many efforts have also been devoted to explore transition metal vanadate favoring multielectron redox per formula unit.[100-102] In 2016, F. Nazar's group reported a microwave-assisted hydrothermal method to synthesize single-crystal $Zn_{0.25}V_2O_5{\cdot}nH_2O$ nanobelts which delivered a superior specific capacity and prolong cyclability.[59] The compound has a double-layer structure with a layer spacing of more than 1 nm. The water molecules and Zn^{2+} serve as "pillars" between interlayer to stabilize the interior structure. HRTEM image proved that the nanobelts exhibit a lattice spacing of 0.537 nm, corresponding to (200) planes. The authors claimed that these planes are parallel to the length of the nanobelts, suggesting that that the *b* axis is the crystal growth direction. The Alshareef's group subsequently reported an ultra-long ZVO nanowires with a porous frame, which display a high energy density when serves as Zn ion cathode materials.[103] The opening framework and multiple oxidation states are the reasons to the performance enhancements. In 2019, Wang *et al.* made a significant improvement in specific capacity.[104] Through a spontaneous phase transition, VOOH hollow nanospheres was converted to reversible $Zn_{0.3}V_2O_5{\cdot}1.5H_2O$ (ZVO) nanoflowers (**Fig. 9**a and Fig. 9b). A remarkable capacity of 426 mAh g^{-1} at

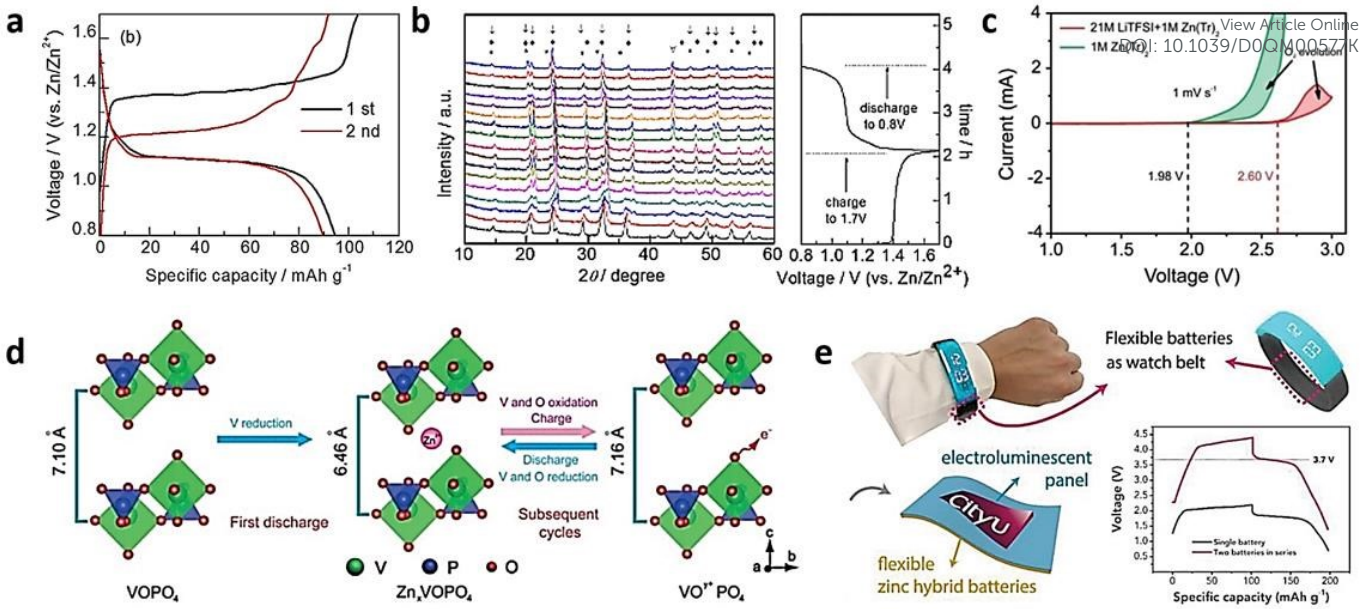

Fig. 11 (a) Galvanostatic charge-discharge curves of $Na_3V_2(PO_4)_3$ electrode. (b) Ex-situ XRD patterns of $Na_3V_2(PO_4)_3$ cathode during reaction processes. Reproduced with permission from ref. 63. Copyright 2016 Elsevier. (c) CV curves of Zn electrodes in different electrolytes. (d) Oxygen and vanadium redox mechanism during charge/discharge processes. Reproduced with permission from ref. 116. Copyright 2019 Wiley-VCH. (e) An exhibition of a wearable electronic watch driven by the flexible Zn//$LiVPO_4F$ batteries. Reproduced with permission from ref. 117. Copyright 2019 WILEY-VCH.

0.2 A g^{-1} and excellent cyclability of 20,000 cycles with 96% of the capacity retained were delivered by ZVO electrode, (Fig. 9c). The activation process at low current density and reassembling of batteries are the key factors of that superior performance. As shown in Fig. 9d, after 10 cycles of activation, the VOOH electrode completely transform to ZVO, which is indicated by the diffraction peak from (001) to (005) planes. More interestingly, the interlayer spacing of ZVO remains almost unchanged during the Zn^{2+} and H^+ intercalation/extraction process (Fig. 9e and Fig. 9f). The author emphasizes that the effects of electrochemical reactions can be reduced to a minimum thanks to the cancellation of two opposite effects which results in a constant interlayer distance throughout the charge/discharge cycle.

Interlayer Mn^{2+}-doped vanadium oxide hybrids are also the research hotspots in cathode materials towards ZIBs. An expanded interlayer spacing manganese hydrated vanadate (MnVO) with connected layers was fabricated by Liu *et al.*[105] Upon discharge at a high current density, Mn^{2+} facilitates the rapid insertion of Zn^{2+}; thus; significantly enhancing the electrochemical performances. An Mn^{2+}-doped vanadium oxide ($Mn_{0.15}V_2O_5{\cdot}nH_2O$) that can work at low temperature (-20 °C) was explored by Li's group in 2020.[58] The narrow direct bandgap enhanced the excitation of the conduction band by carriers, resulting in the increased conductivity. *Ex-situ* XRD patterns show the shift to higher angles during the first discharge, which proved the contraction of the interlayer spacing during Zn^{2+} insertion (**Fig. 10**a). This phenomenon can be attributed to the weakening electrostatic repulsion between connected layers and the improved combination of Zn^{2+} with lattice oxygen and water molecules. While charging, the XRD peaks recovered to the initial position, demonstrating the high reversibility of electrode structure, contributing to the stable cycling performance. The author claimed that the synergistic effect between the intercalated Mn^{2+} ions or water molecules and the layered nanostructures enhanced the electron/ion transport kinetics; thus, improving the structural stability during cycling.

Common transition metals (Fe, Co, Ni, and Cu) can also be combined with vanadium oxides to form vanadates for ZIBs.[106, 107] In 2019, Zhi's group reported a $Co_{0.247}V_2O_5{\cdot}0.944H_2O$ nanobelts with extraordinary capacity (432 mAh g^{-1} at 100 mA g^{-1}) and excellent rate-capacity performance (163 mAh g^{-1} at 10 A g^{-1}).[108] By first-principle calculation, owing to the Co^{2+} intercalation into layers, the absorption energy for Zn^{2+} increased by 0.39 eV compared to the pristine $V_2O_5{\cdot}nH_2O$, resulting in a high working voltage of Zn//$Co_{0.247}V_2O_5{\cdot}0.944H_2O$ system. Subsequently, the high output voltage together with high capacity of $Co_{0.247}V_2O_5{\cdot}0.944H_2O$ results in the outstanding energy density of 458.7 Wh kg^{-1}. Moreover, two new phases of hydrated δ-$Ni_{0.25}V_2O_5$ and δ-$Co_{0.25}V_2O_5$ were fabricated and first utilized for ZIBs by P. Parkin's group recently, which exhibited the outstanding electrochemical performance.[60]

Recently, thanks to the high conductivity of silver, silver vanadate of cathode materials has been gradually reported.[109] The existence of silver nanoparticles is conducive to the pseudo-zinc-air reaction, and at the same time, benefiting the electrochemical performance. In 2019, Wang's group reported an $Ag_2V_4O_{11}$ (AVO) layered structure as cathode materials in ZIBs.[61] Through a simple titration method, the authors firstly confirmed the phase composition of the basic zinc salt (BZS) in the $Zn(CF_3SO_3)_2$-based electrolyte. Experimental results clearly demonstrate the simultaneous formation/decomposition of silver and BZS, further confirming feasible pseudo-zinc-air reaction mode arose on the surface of silver. Moreover, *ex-situ*

XRD analysis further ensures the reversible reaction process of $Zn(H_2O)_6^{2+}$. As shown in Fig. 10b, the capacitive contribution is more than 88% at 0.5 mV s^{-1}, which is beneficial to high-rate performance. Therefore, the AVO cathode exhibits an extraordinary electrochemical performance (capacity retention of 93% at 5 A g^{-1} after 6000 cycles).

3.2.4. Ammonium Vanadates

In the past few years, ammonium vanadates have been reported as an extraordinary cathode for ZIBs.[110, 111] For example, ultrathin $(NH_4)_2V_{10}O_{25}$ nanobelts were fabricated by Wei *et al.* in 2018.[112] With an expanded spacing layer from 1.04 nm to 1.32 nm in *c*-axis along with the facile Zn^{2+} insertion, the electrode delivered an excellent rate performances as well as an outstanding specific energy density up to 225.4 Wh kg^{-1} without structural damage (Fig. 10c). Similarly, $NH_4V_4O_{10}$ with interlayer spacing of 9.8 Å was also reported by Tang *et al*., which delivered impressive electrochemical properties (Fig. 10d).[62] The *ex-situ* XRD results suggested that corresponding interlayer spacing was narrowed during the Zn^{2+} insertion, which can be attributed to the intensive interlayer electrostatic attraction between V_3O_8 layers and inserted Zn^{2+}. Based on some data discussion and analysis, the author summarizes the reaction mechanism can be illustrated in Fig. 10e.

3.3. Vanadium Phosphates

Due to the presence of $[PO_4]$ tetrahedrons and [VO6] octahedrons in the structure, vanadium phosphate usually exhibits robust crystal structures with good structural stability during the ions insertion/extraction compared to other vanadium-based electrodes.[113] Few of vanadium phosphates possesses the layered structure, such as $VOPO_4$. However, the majority of the vanadium phosphates have the three-dimensional open framework structure which are connected by $[VO_6]$ octahedron and $[PO_4]$ tetrahedron through a shared corner. Due to $[VO_6]$ octahedrons that are separated by $[PO_4]$ tetrahedrons and are isolated from each other, vanadium phosphates usually attain poor electron transfer. The most effective modification method to overcome that has been nanostructuring and conductive coating.

Oxygen redox reactions in ZIBs usually take place in vanadium-based compound, leading to an obvious enhancement of the electrochemical activity at the oxygen center. Increasing the electron density of oxygen atoms by reducing the covalent state of V-O is an effective strategy. Among vanadium oxides and vanadates, only the V_xO_y polyhedron has abundant V-O covalent.[114] P-O covalent displays weaker bonding energy as compared to V-O covalent. Consequently, the importation of P-O covalent in the V_xO_y polyhedron layer will increase the electron density of oxygen. Owing to the merits of high output voltage, stabilized interior nanostructure as well as fast ion diffusion coefficient, many vanadium phosphates, such as $Zn_{0.4}VOPO_4{\cdot}0.8H_2O$, have been widely put into practice as cathode materials for ZIBs.[115]

Thanks to the stable 3D Na^+ superionic conductor structure, $Na_3V_2(PO_4)_3$ (NVP) has been widely studied as cathode materials for ZIBs. For example, in 2016, Li's group prepared the $Na_3V_2(PO_4)_3$ as the ZIBs cathode materials.[63] Graphene-like carbon was used for the purpose of overcoming the weakness of poor conductivity. This special cathode delivered a remarkable capacity and good cyclability in a 0.5 M $Zn(CH_3COO)_2$ electrolyte. Importantly, the $Zn//Na_3V_2(PO_4)_3$ system displays high voltage platform (about 1.1 V while discharging) (**Fig. 11**a). The *ex-situ* XRD were employed to explore the reaction mechanism of $Na_3V_2(PO_4)_3$ during the (de)intercalation process of Zn^{2+}, which demonstrate marginal difference from the other cathodes that we have discussed above. During the first cycle of charging process, two Na^+ were extracted from the $Na_3V_2(PO_4)_3$ cathode which transform to a new phase of $NaV_2(PO_4)_3$. In the following cycles, Zn^{2+} exhibit continuous insertion and extraction behavior in $Na_3V_2(PO_4)_3$ cathode without the Na^+ extraction (Fig. 11b). According to the Rietveld-refined XRD results, shrunk lattice constant was seen, which is attributed to the formation of new vacancies or the higher charge current density during Zn^{2+} intercalation. Moreover, the authors claimed that Zn^{2+} may occupy 6b and 18e sites at the same time, and then change the occupied sites during insertion. From the *ex-situ* XPS spectra, during the first cycle of charging process, V^{3+} is oxidized into V^{4+}. In the subsequent discharging procedure, V^{4+} is reduced back to V^{3+}, while part of Zn^{2+} ions are irreversibly inserted.

$VOPO_4$, an atypical layered structure, is connected to the PO_4 tetrahedron by a common angle VO_6 octahedron. A layered $VOPO_4$ cathode was fabricated by Niu's group, which delivered a reversible oxygen redox electrochemical performance at a high output voltage region.[116] An additional capacity of about 27% was provided by the redox process, and the averaged operating voltage was soared to approximately 1.56 V (doubled those of traditional vanadium-based ZIBs), thereby boosting the energy density by 36%. More importantly, in this system, the authors use a mixture of LiTFSI and $Zn(Tr)_2$ as the electrolyte to ensure high working voltage and inhibit the decomposition of $VOPO_4$ during reaction (Fig. 11c). By the XPS analysis of $VOPO_4$ after cycling, the Zn^{2+} extraction and oxidation of V and P were not found, indicating that the platform of high voltage region should be arose from the oxidation of oxygen. The XANES results further prove the oxygen redox process should be occurred at the high-voltage region. The above discussion could summarize the reaction mechanism contributed to the remarkable energy density (217 Wh kg^{-1}) of $VOPO_4$ electrode (Fig. 11d).

A flexible solid-state aqueous ZIBs using "scarf-blanket" hierarchically structured $LiVPO_4F$ as cathode was fabricated by Liu *et al.*[117] Because of the poor electronic conductivity of $LiVPO_4F$, CNTs and PPy were employed to largely boost the electrochemical performances. The electrode displayed a high-voltage plateau of about 1.9 V in aqueous ZIBs; hence, a superior specific capacity and excellent energy density (235.6 Wh kg^{-1}) were seen. When $LiVPO_4F$ was applied to un-sealed flexible battery (Fig. 11e), remarkable electrochemical properties were delivered at various bending states with a stabilized output voltage of 3.7 V at 800 mA g^{-1}.

4. Summary and Prospects

View Article Online
DOI: 10.1039/D0QM00577K

The development of Zn ions storage device is driven by the innovation in cathode materials. Vanadium-based materials with a large family members, diverse compositions, structures and characteristics, have provided great potentials towards ZIBs. In this review, we have comprehensively summarized most recent advances of vanadium-based nanomaterials as cathode materials for ZIBs, classified into vanadium oxide, vanadates, and vanadium phosphates. Inserted metal ions and water molecular between layers could act as "pillars" to alter the layer spacing and stabilize cathode structure, accelerating the migration rate of Zn^{2+} insertion/extraction into vanadium-based cathodes. More importantly, apart from the traditional insertion/extraction of Zn^{2+}, the simultaneous-insertion of H^+ and Zn^{2+} was also discovered. The involvement of H^+ gives rise to the rapid kinetics; thus, enhancing the capacity and cycling performances.

Despite the impressive progress already reported, vanadium-based cathode is still far from practical applications; and therefore, greater efforts need to be made to improve cycling stability and capacity:

1) Vanadium-based compounds usually show a low operating voltage in zinc ion battery system (usually less than 2 V), which seriously limits the energy density of vanadium-based ZIBs. By incorporating electron-absorbing groups into vanadium-based cathode, the average operating voltage can be increased. Therefore, further study should concentrate on high working voltage and high specific capacity, so as to further realize high energy density of ZIBs.

2) Designing the hierarchical structure of the electrode is considered to be a promising approach since abundant porous channels for ion transfer and high vibrational density could be delivered, thus further improving the volumetric energy density.

3) During rapid insertion/extraction of Zn^{2+}, the layered structure of vanadium-based nanomaterials may be impaired. Therefore, interlayered insertion of metal ions or bonded water is an effective method to enhance the interlaminar attraction and further strengthen the layered structure.

4) Vanadium-based ZIBs also exhibit a controversial reaction mechanism. Electrode materials are essentially undergoing phase transition during the reaction process. In addition to inhibiting the insertion of Zn^{2+}, the metal ions inserted between the layers will also cause a phase change. The insertion of metal ions results in phase transition, and it depends on the type/number of metal ions. Thus, it is necessary to further obtain the relationship between inserted metal ions and the crystal structure/electrochemical performance. At the same time, the reaction mechanism of water molecules between layers also needs further exploration.

5) The conductivity of vanadium-based electrodes should also be improved to facilitate the charge transfer during the insertion/extraction. In addition, the morphological design with a larger number of exposed active areas has also proved to be an effective means to enhance the electrode activity, along with the combination of conductive materials.

6) The weakly acidic electrolyte which slowly dissolves vanadium or vanadium oxide, might be the reason for the decline in cycle efficiency. This issue has yet to be properly discussed. Electrolyte optimization is a promising research direction that need a lot more attention.

Conflicts of interest

There are no conflicts to declare.

Acknowledgments

This work was financially supported by the National Natural Science Foundation of China (51872139, 51902158), the NSF of Jiangsu Province (BK20170045), the Recruitment Program of Global Experts (1211019), the "Six Talent Peak" Project of Jiangsu Province (XCL-043, XCL-021), and Natural Science Foundation of Jiangsu Higher Education Institutions (19KJB430002). Q. Y. acknowledges Singapore MOE AcRF Teir 1 2017-T1-02-009, Tier 2 under Grant Nos. 2017-T2-2-069 and National Research Foundation of Singapore (NRF) Investigatorship, award Number NRF2016NRF-NRFI001-22.

Notes and references

1 S. Chu and A. Majumdar, Opportunities and Challenges for a Sustainable Energy Future, *Nature*, 2012, **488**, 294–303.
2 S. Chu, Y. Cui and N. Liu, The Path towards Sustainable Energy, *Nat. Mater.*, 2017, **16**, 16–22.
3 K. Rui, G. Zhao, M. Lao, P. Cui, X. Zheng, X. Zheng, J. Zhu, W. Huang, S. X. Dou and W. Sun, Direct Hybridization of Noble Metal Nanostructures on 2D Metal–Organic Framework Nanosheets to Catalyze Hydrogen Evolution, *Nano Lett.*, 2019, **19**, 8447–8453.
4 L. Pan, J. Dong, D. Yi, Y. Yang and X. Wang, Recent Advances in Atomic-Scale Storage Mechanism Studies of Two-Dimensional Nanomaterials for Rechargeable Batteries Beyond Li-ion, *Chem. Res. Chin. Univ.*, 2020, **36**, 560–583.
5 C. Yang, J. Chai, Z. Wang, Y. Xing, J. Peng and Q. Yan, Recent Progress on Bismuth-Based Nanomaterials for Electrocatalytic Carbon Dioxide Reduction, *Chem. Res. Chin. Univ.*, 2020, **36**, 410–419.
6 H. Yu, Y. G. So, Y. Ren, T. Wu, G. Guo, R. Xiao, J. Lu, H. Li, Y. Yang, H. Zhou, R. Wang, K. Amine and Y. Ikuhara, Temperature-Sensitive Structure Evolution of Lithium-Manganese-Rich Layered Oxides for Lithium-Ion Batteries, *J. Am. Chem. Soc.*, 2018, **140**, 15279–15289.
7 Z. Yang, J. Zhang, M. C. W. Kintner-Meyer, X. Lu, D. Choi, J. P. Lemmon and J. Liu, Electrochemical Energy Storage for Green Grid, *Chem. Rev.*, 2011, **111**, 3577–3613.
8 M. Armand and J. M. Tarascon, Building Better Batteries, *Nature*, 2008, **451**, 652–657.
9 W. Wang, T. Wang, X. Fan, C. Zhang, J. Hu, H. Chen, Z. Fang, J. Yan and B. Liu, Freeze-Drying-Assisted Synthesis of Mesoporous $CoMoO_4$ Nanosheets as Anode Electrode Material for Enhanced Lithium Batteries, *Chem. Res. Chin. Univ.*, 2019, **35**, 261–270.
10 D. He, B. Wang, T. Wu, H. Su, X. Zhang, Y. Ren, G. L. Xu, Z. Liu, J. Wang, K. Amine and H. Yu, TiO_2 Nanocrystal-Framed

Li_2TiSiO_5 Platelets for Low-Voltage Lithium Battery Anode, *Adv. Funct. Mater.*, 2020, DOI: 10.1002/adfm.2020019092001909.

11 V. Palomares, P. Serras, I. Villaluenga, K. B. Hueso, J. Carretero-González and T. Rojo, Na-Ion Batteries, Recent Advances and Present Challenges to Become Low Cost Energy Storage Systems, *Energy Environ. Sci.*, 2012, **5**, 5884–5901.

12 N. Yabuuchi, K. Kubota, M. Dahbi and S. Komaba, Research Development on Sodium-Ion Batteries, *Chem. Rev.*, 2014, **114**, 11636–11682.

13 D. Kundu, E. Talaie, V. Duffort and L. F. Nazar, The Emerging Chemistry of Sodium Ion Batteries for Electrochemical Energy Storage, *Angew. Chem. Int. Ed.*, 2015, **54**, 3431–3448.

14 W. Luo, J. Wan, B. Ozdemir, W. Bao, Y. Chen, J. Dai, H. Lin, Y. Xu, F. Gu, V. Barone and L. Hu, Potassium Ion Batteries with Graphitic Materials, *Nano Lett.*, 2015, **15**, 7671–7677.

15 Z. Jian, W. Luo and X. Ji, Carbon Electrodes for K-Ion Batteries, *J. Am. Chem. Soc.*, 2015, **137**, 11566–11569.

16 H. D. Yoo, Y. Liang, H. Dong, J. Lin, H. Wang, Y. Liu, L. Ma, T. Wu, Y. Li, Q. Ru, Y. Jing, Q. An, W. Zhou, J. Guo, J. Lu, S. T. Pantelides, X. Qian and Y. Yao, Fast Kinetics of Magnesium Monochloride Cations in Interlayer-Expanded Titanium Disulfide for Magnesium Rechargeable Batteries, *Nat. Commun.*, 2017, **8**, 339.

17 Z. Jian, Z. Xing, C. Bommier, Z. Li and X. Ji, Hard Carbon Microspheres: Potassium-Ion Anode Versus Sodium-Ion Anode, *Adv. Energy Mater.*, 2016, **6**, 1501874.

18 L. Xu, J. Li, Y. Li, P. Cai, C. Liu, G. Zou, H. Hou, L. Huang and X. Ji, Nitrogen-doped Carbon Coated $Na_3V_2(PO_4)_3$ with Superior Sodium Storage Capability, *Chem. Res. Chin. Univ.*, 2020, **36**, 459–466.

19 M. Ghosh, V. Vijayakumar and S. Kurungot, Dendrite Growth Suppression by Zn^{2+}-Integrated Nafion Ionomer Membranes: Beyond Porous Separators toward Aqueous Zn/V_2O_5 Batteries with Extended Cycle Life, *Energy Technol.*, 2019, **7**, 1900442.

20 Y. Li, Z. Huang, P. K. Kalambate, Y. Zhong, Z. Huang, M. Xie, Y. Shen and Y. Huang, V_2O_5 Nanopaper as a Cathode Material with High Capacity and Long Cycle Life for Rechargeable Aqueous Zinc-Ion Battery, *Nano Energy*, 2019, **60**, 752–759.

21 H. Qin, L. Chen, L. Wang, X. Chen and Z. Yang, V_2O_5 Hollow Spheres as High Rate and Long Life Cathode for Aqueous Rechargeable Zinc Ion Batteries, *Electrochim. Acta*, 2019, **306**, 307–316.

22 D. Xu, H. Wang, F. Li, Z. Guan, R. Wang, B. He, Y. Gong and X. Hu, Conformal Conducting Polymer Shells on V_2O_5 Nanosheet Arrays as a High-Rate and Stable Zinc-Ion Battery Cathode, *Adv. Mater. Interfaces*, 2019, **6**, 1801506.

23 S. Takayuki, H. Masakazu and Y. Takakazu, Zinc-Manganese Dioxide Galvanic Cell Using Zinc Sulphate as Electrolyte. Rechargeability of the cell, *J. Appl. Electrochem.*, 1988, **18**, 521–526.

24 Y. Zhang, K. Rui, A. Huang, Y. Ding, K. Hu, W. Shi, X. Cao, H. Lin, J. Zhu and W. Huang, Stereoassembled V_2O_5@FeOOH Hollow Architectures with Lithiation Volumetric Strain Self-Reconstruction for Lithium-Ion Storage, *Research*, 2020, **2020**, 2360796.

25 M. M. Huie, D. C. Bock, E. S. Takeuchi, A. C. Marschilok and K. J. Takeuchi, Cathode Materials for Magnesium and Magnesium-Ion Based Batteries, *Coord. Chem. Rev.*, 2015, **287**, 15–27.

26 Q. An, Q. Wei, P. Zhang, J. Sheng, K. M. Hercule, F. Lv, Q. Wang, X. Wei and L. Mai, Three-Dimensional Interconnected Vanadium Pentoxide Nanonetwork Cathode for High-Rate Long-Life Lithium Batteries, *Small*, 2015, **11**, 2654–2660.

27 Y. Zhao, C. Han, J. Yang, J. Su, X. Xu, S. Li, L. Xu, R. Fang, H. Jiang, X. Zou, B. Song, L. Mai and Q. Zhang, Stable Alkali Metal Ion Intercalation Compounds as Optimized Metal Oxide Nanowire Cathodes for Lithium Batteries, *Nano Lett.*, 2015, **15**, 2180–2185.

28 Q. An, P. Zhang, Q. Wei, L. He, F. Xiong, J. Sheng, Q. Wang and L. Mai, Top-Down Fabrication of Three-Dimensional Porous V_2O_5 Hierarchical Microplates with Tunable Porosity for Improved Lithium Battery Performance, *J. Mater. Chem. A*, 2014, **2**, 3297–3302.

29 F. R. McLarnon, The Secondary Alkaline Zinc Electrode, *J. Electrochem. Soc.*, 1991, **138**, 645.

30 N. Zhang, F. Cheng, J. Liu, L. Wang, X. Long, X. Liu, F. Li and J. Chen, Rechargeable Aqueous Zinc-Manganese Dioxide Batteries with High Energy and Power Densities, *Nat. Commun.*, 2017, **8**, 405.

31 Y. Shao, M. F. El-Kady, J. Sun, Y. Li, Q. Zhang, M. Zhu, H. Wang, B. Dunn and R. B. Kaner, Design and Mechanisms of Asymmetric Supercapacitors, *Chem. Rev.*, 2018, **118**, 9233–9280.

32 Y. Wang and Y. Xia, Recent Progress in Supercapacitors: From Materials Design to System Construction, *Adv. Mater.*, 2013, **25**, 5336–5342.

33 H. Jiang, J. Ma and C. Li, Mesoporous Carbon Incorporated Metal Oxide Nanomaterials as Supercapacitor Electrodes, *Adv. Mater.*, 2012, **24**, 4197–4202.

34 J. Yan, Q. Wang, T. Wei and Z. Fan, Recent Advances in Design and Fabrication of Electrochemical Supercapacitors with High Energy Densities, *Adv. Energy Mater.*, 2014, **4**, 1300816.

35 C. Xu, B. Li, H. Du and F. Kang, Energetic Zinc Ion Chemistry: the Rechargeable Zinc Ion Battery, *Angew. Chem. Int. Ed.*, 2012, **51**, 933–935.

36 D. Chen, X. Rui, Q. Zhang, H. Geng, L. Gan, W. Zhang, C. Li, S. Huang and Y. Yu, Persistent Zinc-Ion Storage in Mass-Produced V_2O_5 Architectures, *Nano Energy*, 2019, **60**, 171–178.

37 Y. Tian, Y. An, H. Wei, C. Wei, Y. Tao, Y. Li, B. Xi, S. Xiong, J. Feng and Y. Qian, Micron-Sized Nanoporous Vanadium Pentoxide Arrays for High-Performance Gel Zinc-Ion Batteries and Potassium Batteries, *Chem. Mater.*, 2020, **32**, 4054–4064.

38 Q. Li, Q. Zhang, C. Liu, Z. Zhou, C. Li, B. He, P. Man, X. Wang and Y. Yao, Anchoring V_2O_5 Nanosheets on Hierarchical Titanium Nitride Nanowire Arrays to Form Core–Shell Heterostructures as a Superior Cathode for High-Performance Wearable Aqueous Rechargeable Zinc-Ion Batteries, *J. Mater. Chem. A*, 2019, **7**, 12997–13006.

View Article Online
DOI: 10.1039/D0QM00577K

39 X. Chen, L. Wang, H. Li, F. Cheng and J. Chen, Porous V_2O_5 Nanofibers as Cathode Materials for Rechargeable Aqueous Zinc-Ion Batteries, *J. Energy Chem.*, 2019, **38**, 20–25.

40 J. Zhou, L. Shan, Z. Wu, X. Guo, G. Fang and S. Liang, Investigation of V_2O_5 as a Low-Cost Rechargeable Aqueous Zinc Ion Battery Cathode, *Chem. Commun.*, 2018, **54**, 4457–4460.

41 N. Zhang, Y. Dong, M. Jia, X. Bian, Y. Wang, M. Qiu, J. Xu, Y. Liu, L. Jiao and F. Cheng, Rechargeable Aqueous Zn–V_2O_5 Battery with High Energy Density and Long Cycle Life, *ACS Energy Lett.*, 2018, **3**, 1366–1372.

42 B. He, Z. Zhou, P. Man, Q. Zhang, C. Li, L. Xie, X. Wang, Q. Li and Y. Yao, V_2O_5 Nanosheets Supported on 3D N-Doped Carbon Nanowall Arrays as an Advanced Cathode for High Energy and High Power Fiber-Shaped Zinc-Ion Batteries, *J. Mater. Chem. A*, 2019, **7**, 12979–12986.

43 P. Hu, T. Zhu, J. Ma, C. Cai, G. Hu, X. Wang, Z. Liu, L. Zhou and L. Mai, Porous V_2O_5 Microspheres: A High-Capacity Cathode Material for Aqueous Zinc-Ion Batteries, *Chem. Commun.*, 2019, **55**, 8486–8489.

44 P. Senguttuvan, S.-D. Han, S. Kim, A. L. Lipson, S. Tepavcevic, T. T. Fister, I. D. Bloom, A. K. Burrell and C. S. Johnson, A High Power Rechargeable Nonaqueous Multivalent Zn/V_2O_5 Battery, *Adv. Energy Mater.*, 2016, **6**, 1600826.

45 N. Zhang, M. Jia, Y. Dong, Y. Wang, J. Xu, Y. Liu, L. Jiao and F. Cheng, Hydrated Layered Vanadium Oxide as a Highly Reversible Cathode for Rechargeable Aqueous Zinc Batteries, *Adv. Funct. Mater.*, 2019, **29**, 1807331.

46 L. Chen, Z. Yang and Y. Huang, Monoclinic VO_2(D) Hollow Nanospheres with Super-Long Cycle Life for Aqueous Zinc Ion Batteries, *Nanoscale*, 2019, **11**, 13032–13039.

47 J. Ding, Z. Du, L. Gu, B. Li, L. Wang, S. Wang, Y. Gong and S. Yang, Ultrafast Zn^{2+} Intercalation and Deintercalation in Vanadium Dioxide, *Adv. Mater.*, 2018, **30**, 1800762.

48 D. Kundu, S. Hosseini Vajargah, L. Wan, B. Adams, D. Prendergast and L. F. Nazar, Aqueous vs. Nonaqueous Zn-Ion Batteries: Consequences of the Desolvation Penalty at the Interface, *Energy Environ. Sci.*, 2018, **11**, 881–892.

49 C. Shen, X. Li, N. Li, K. Xie, J. G. Wang, X. Liu and B. Wei, Graphene-Boosted, High-Performance Aqueous Zn-Ion Battery, *ACS Appl. Mater. Interfaces*, 2018, **10**, 25446–25453.

50 J. Lai, H. Zhu, X. Zhu, H. Koritala and Y. Wang, Interlayer-Expanded $V_6O_{13}{\cdot}nH_2O$ Architecture Constructed for an Advanced Rechargeable Aqueous Zinc-Ion Battery, *ACS Appl. Energy Mater.*, 2019, **2**, 1988–1996.

51 L. Qian, T. Wei, K. Ma, G. Yang and C. Wang, Boosting the Cyclic Stability of Aqueous Zinc-Ion Battery Based on Al-Doped $V_{10}O_{24}{\cdot}12H_2O$ Cathode Materials, *ACS Appl. Mater. Interfaces*, 2019, **11**, 20888–20894.

52 Y. Ding, Y. Peng, S. Chen, X. Zhang, Z. Li, L. Zhu, L. E. Mo and L. Hu, Hierarchical Porous Metallic V_2O_3@C for Advanced Aqueous Zinc-Ion Batteries, *ACS Appl. Mater. Interfaces*, 2019, **11**, 44109–44117.

53 M. H. Alfaruqi, V. Mathew, J. Song, S. Kim, S. Islam, D. T. Pham, J. Jo, S. Kim, J. P. Baboo, Z. Xiu, K.-S. Lee, Y.-K. Sun and J. Kim, Electrochemical Zinc Intercalation in Lithium Vanadium Oxide: A High-Capacity Zinc-Ion Battery Cathode, *Chem. Mater.*, 2017, **29**, 1684–1694.

54 P. He, G. Zhang, X. Liao, M. Yan, X. Xu, Q. An, J. Liu and L. Mai, Sodium Ion Stabilized Vanadium Oxide Nanowire Cathode for High-Performance Zinc-Ion Batteries, *Adv. Energy Mater.*, 2018, **8**, 1702463.

55 W. Yang, L. Dong, W. Yang, C. Xu, G. Shao and G. Wang, 3D Oxygen-Defective Potassium Vanadate/Carbon Nanoribbon Networks as High-Performance Cathodes for Aqueous Zinc-Ion Batteries, *Small Methods*, 2019, **4**, 1900670.

56 F. Ming, H. Liang, Y. Lei, S. Kandambeth, M. Eddaoudi and H. N. Alshareef, Layered $Mg_xV_2O_5{\cdot}nH_2O$ as Cathode Material for High-Performance Aqueous Zinc Ion Batteries, *ACS Energy Lett.*, 2018, **3**, 2602–2609.

57 C. Xia, J. Guo, P. Li, X. Zhang and H. N. Alshareef, Highly Stable Aqueous Zinc-Ion Storage Using a Layered Calcium Vanadium Oxide Bronze Cathode, *Angew. Chem. Int. Ed.*, 2018, **57**, 3943–3948.

58 H. Geng, M. Cheng, B. Wang, Y. Yang, Y. Zhang and C. C. Li, Electronic Structure Regulation of Layered Vanadium Oxide via Interlayer Doping Strategy toward Superior High-Rate and Low-Temperature Zinc-Ion Batteries, *Adv. Funct. Mater.*, 2019, **30**, 1907684.

59 D. Kundu, B. D. Adams, V. Duffort, S. H. Vajargah and L. F. Nazar, A High-Capacity and Long-Life Aqueous Rechargeable Zinc Battery Using a Metal Oxide Intercalation Cathode, *Nat. Energy*, 2016, **1**, 16119.

60 J. Li, K. McColl, X. Lu, S. Sathasivam, H. Dong, L. Kang, Z. Li, S. Zhao, A. G. Kafizas, R. Wang, D. J. L. Brett, P. R. Shearing, F. Corà, G. He, C. J. Carmalt and I. P. Parkin, Multi-Scale Investigations of δ-$Ni_{0.25}V_2O_5{\cdot}nH_2O$ Cathode Materials in Aqueous Zinc-Ion Batteries, *Adv. Energy Mater.*, 2020, **10**, 2000058.

61 Q. Li, Y. Liu, K. Ma, G. Yang and C. Wang, In Situ Ag Nanoparticles Reinforced Pseudo-Zn-Air Reaction Boosting $Ag_2V_4O_{11}$ as High-Performance Cathode Material for Aqueous Zinc-Ion Batteries, *Small Methods*, 2019, **3**, 1900637.

62 B. Tang, J. Zhou, G. Fang, F. Liu, C. Zhu, C. Wang, A. Pan and S. Liang, Engineering the Interplanar Spacing of Ammonium Vanadates as a High-Performance Aqueous Zinc-Ion Battery Cathode, *J. Mater. Chem. A*, 2019, **7**, 940–945.

63 G. Li, Z. Yang, Y. Jiang, C. Jin, W. Huang, X. Ding and Y. Huang, Towards Polyvalent Ion Batteries: A Zinc-Ion Battery Based on NASICON Structured $Na_3V_2(PO_4)_3$, *Nano Energy*, 2016, **25**, 211–217.

64 P. Hu, M. Yan, T. Zhu, X. Wang, X. Wei, J. Li, L. Zhou, Z. Li, L. Chen and L. Mai, Zn/V_2O_5 Aqueous Hybrid-Ion Battery with High Voltage Platform and Long Cycle Life, *ACS Appl. Mater. Interfaces*, 2017, **9**, 42717–42722.

65 F. Liu, Z. Chen, G. Fang, Z. Wang, Y. Cai, B. Tang, J. Zhou and S. Liang, V_2O_5 Nanospheres with Mixed Vanadium Valences as High Electrochemically Active Aqueous Zinc-Ion Battery Cathode, *Nano-Micro Lett.*, 2019, **11**, 25.

66 J. Zhao, H. Ren, Q. Liang, D. Yuan, S. Xi, C. Wu, W. Manalastas, J. Ma, W. Fang, Y. Zheng, C.-F. Du, M. Srinivasan and Q. Yan, High-Performance Flexible Quasi-Solid-State Zinc-Ion

Batteries with Layer-Expanded Vanadium Oxide Cathode and Zinc/Stainless Steel Mesh Composite Anode, *Nano Energy*, 2019, **62**, 94−102.

67 L. Chen, Z. Yang, F. Cui, J. Meng, H. Chen and X. Zeng, Enhanced Rate and Cycling Performances of Hollow V_2O_5 Nanospheres for Aqueous Zinc Ion Battery Cathode, *Appl. Surf. Sci.*, 2020, **507**, 145137.

68 M. S. Javed, H. Lei, Z. Wang, B.-t. Liu, X. Cai and W. Mai, 2D V_2O_5 Nanosheets as a Binder-Free High-Energy Cathode for Ultrafast Aqueous and Flexible Zn-Ion Batteries, *Nano Energy*, 2020, **70**, 104573.

69 B. Yin, S. Zhang, K. Ke, T. Xiong, Y. Wang, B. K. D. Lim, W. S. V. Lee, Z. Wang and J. Xue, Binder-Free V_2O_5/CNT Paper Electrode for High Rate Performance Zinc Ion Battery, *Nanoscale*, 2019, **11**, 19723−19728.

70 M. D. Wei, H. Sugihara, I. Honma, M. Ichihara and H. S. Zhou, A New Metastable Phase of Crystallized $V_2O_4{\cdot}0.25H_2O$ Nanowires: Synthesis and Electrochemical Measurements, *Adv. Mater.*, 2005, **17**, 2964−2969.

71 F. Cui, J. Zhao, D. Zhang, Y. Fang, F. Hu and K. Zhu, VO_2(B) Nanobelts and Reduced Graphene Oxides Composites as Cathode Materials for Low-Cost Rechargeable Aqueous Zinc Ion Batteries, *Chem. Eng. J.*, 2020, **390**, 124118.

72 D. Chao, C. Zhu, X. Xia, J. Liu, X. Zhang, J. Wang, P. Liang, J. Lin, H. Zhang, Z. X. Shen and H. J. Fan, Graphene Quantum Dots Coated VO_2 Arrays for Highly Durable Electrodes for Li and Na Ion Batteries, *Nano Lett.*, 2015, **15**, 565−573.

73 Z. Li, S. Ganapathy, Y. Xu, Z. Zhou, M. Sarilar and M. Wagemaker, Mechanistic Insight into the Electrochemical Performance of Zn/VO_2 Batteries with an Aqueous $ZnSO_4$ Electrolyte, *Adv. Energy Mater.*, 2019, **9**, 1900237.

74 W. Sun, F. Wang, S. Hou, C. Yang, X. Fan, Z. Ma, T. Gao, F. Han, R. Hu, M. Zhu and C. Wang, Zn/MnO_2 Battery Chemistry With H^+ and Zn^{2+} Coinsertion, *J. Am. Chem. Soc.*, 2017, **139**, 9775−9778.

75 H. Pan, Y. Shao, P. Yan, Y. Cheng, K. S. Han, Z. Nie, C. Wang, J. Yang, X. Li, P. Bhattacharya, K. T. Mueller and J. Liu, Reversible Aqueous Zinc/Manganese Oxide Energy Storage from Conversion Reactions, *Nat. Energy*, 2016, **1**, 16039.

76 T. Wei, Q. Li, G. Yang and C. Wang, An Electrochemically Induced Bilayered Structure Facilitates Long-Life Zinc Storage of Vanadium Dioxide, *J. Mater. Chem. A*, 2018, **6**, 8006−8012.

77 J.-S. Park, J. H. Jo, Y. Aniskevich, A. Bakavets, G. Ragoisha, E. Streltsov, J. Kim and S.-T. Myung, Open-Structured Vanadium Dioxide as an Intercalation Host for Zn Ions: Investigation by First-Principles Calculation and Experiments, *Chem. Mater.*, 2018, **30**, 6777−6787.

78 X. Dai, F. Wan, L. Zhang, H. Cao and Z. Niu, Freestanding Graphene/VO_2 Composite Films for Highly Stable Aqueous Zn-Ion Batteries with Superior Rate Performance, *Energy Storage Mater.*, 2019, **17**, 143−150.

79 R. Li, X. Yu, X. Bian and F. Hu, Preparation and Electrochemical Performance of VO_2(A) Hollow Spheres as a Cathode for Aqueous Zinc Ion Batteries, *RSC Adv.*, 2019, **9**, 35117−35123.

80 C. Zhang, H. Song, C. Zhang, C. Liu, Y. Liu and G. Cao, Interface Reduction Synthesis of $H_2V_3O_8$ Nanobelts−Graphene for High-Rate Li-Ion Batteries, *J. Phys. Chem. C*, 2015, **119**, 11391−11399.

81 Z. Cao, H. Chu, H. Zhang, Y. Ge, R. Clemente, P. Dong, L. Wang, J. Shen, M. Ye and P. M. Ajayan, An in situ Electrochemical Oxidation Strategy for Formation of Nanogrid-Shaped $V_3O_7{\cdot}H_2O$ with Enhanced Zinc Storage Properties, *J. Mater. Chem. A*, 2019, **7**, 25262−25267.

82 P. He, Y. Quan, X. Xu, M. Yan, W. Yang, Q. An, L. He and L. Mai, High-Performance Aqueous Zinc-Ion Battery Based on Layered $H_2V_3O_8$ Nanowire Cathode, *Small*, 2017, **13**, 1702551.

83 J. Shin, D. S. Choi, H. J. Lee, Y. Jung and J. W. Choi, Hydrated Intercalation for High-Performance Aqueous Zinc Ion Batteries, *Adv. Energy Mater.*, 2019, **9**, 1900083.

84 M. Liao, J. Wang, L. Ye, H. Sun, Y. Wen, C. Wang, X. Sun, B. Wang and H. Peng, A Deep-Cycle Aqueous Zinc-Ion Battery Containing an Oxygen-Deficient Vanadium Oxide Cathode, *Angew. Chem. Int. Ed.*, 2020, **59**, 2293−2298.

85 T. Wei, Q. Li, G. Yang and C. Wang, High-Rate and Durable Aqueous Zinc Ion Battery Using Dendritic $V_{10}O_{24}{\cdot}12H_2O$ Cathode Material with Large Interlamellar Spacing, *Electrochim. Acta*, 2018, **287**, 60−67.

86 W. Liu, L. Dong, B. Jiang, Y. Huang, X. Wang, C. Xu, Z. Kang, J. Mou and F. Kang, Layered Vanadium Oxides with Proton and Zinc Ion Insertion for Zinc Ion Batteries, *Electrochim. Acta*, 2019, **320**, 134565.

87 H. Luo, B. Wang, F. Wang, J. Yang, F. Wu, Y. Ning, Y. Zhou, D. Wang, H. Liu and S. Dou, Anodic Oxidation Strategy toward Structure-Optimized V_2O_3 Cathode via Electrolyte Regulation for Zn-Ion Storage, *ACS Nano*, 2020, **14**, 7328−7337.

88 B. Sambandam, V. Soundharrajan, S. Kim, M. H. Alfaruqi, J. Jo, S. Kim, V. Mathew, Y.-k. Sun and J. Kim, $K_2V_6O_{16}{\cdot}2.7H_2O$ Nanorod Cathode: An Advanced Intercalation System for High Energy Aqueous Rechargeable Zn-Ion Batteries, *J. Mater. Chem. A*, 2018, **6**, 15530−15539.

89 Y. Yang, Y. Tang, G. Fang, L. Shan, J. Guo, W. Zhang, C. Wang, L. Wang, J. Zhou and S. Liang, Li^+ Intercalated $V_2O_5{\cdot}nH_2O$ with Enlarged Layer Spacing and Fast Ion Diffusion as an Aqueous Zinc-Ion Battery Cathode, *Energy Environ. Sci.*, 2018, **11**, 3157−3162.

90 M. Du, C. Liu, F. Zhang, W. Dong, X. Zhang, Y. Sang, J. J. Wang, Y. G. Guo, H. Liu and S. Wang, Tunable Layered $(Na,Mn)V_8O_{20}{\cdot}nH_2O$ Cathode Material for High-Performance Aqueous Zinc Ion Batteries, *Adv. Sci.*, 2020, DOI: 10.1002/advs.2020000832000083.

91 S. Islam, M. H. Alfaruqi, B. Sambandam, D. Y. Putro, S. Kim, J. Jo, S. Kim, V. Mathew and J. Kim, A New Rechargeable Battery Based on a Zinc Anode and a NaV_6O_{15} Nanorod Cathode, *Chem. Commun.*, 2019, **55**, 3793−3796.

92 S. J. Kim, C. R. Tang, G. Singh, L. M. Housel, S. Yang, K. J. Takeuchi, A. C. Marschilok, E. S. Takeuchi and Y. Zhu, New Insights into the Reaction Mechanism of Sodium Vanadate for an Aqueous Zn Ion Battery, *Chem. Mater.*, 2020, **32**, 2053−2060.

93 V. Soundharrajan, B. Sambandam, S. Kim, M. H. Alfaruqi, D. Y. Putro, J. Jo, S. Kim, V. Mathew, Y. K. Sun and J. Kim, $Na_2V_6O_{16}{\cdot}3H_2O$ Barnesite Nanorod: An Open Door to Display a Stable and High Energy for Aqueous Rechargeable Zn-Ion Batteries as Cathodes, *Nano Lett.*, 2018, **18**, 2402−2410.

94 P. Hu, T. Zhu, X. Wang, X. Wei, M. Yan, J. Li, W. Luo, W. Yang, W. Zhang, L. Zhou, Z. Zhou and L. Mai, Highly Durable $Na_2V_6O_{16}{\cdot}1.63H_2O$ Nanowire Cathode for Aqueous Zinc-Ion Battery, *Nano Lett.*, 2018, **18**, 1758−1763.

95 F. Wan, L. Zhang, X. Dai, X. Wang, Z. Niu and J. Chen, Aqueous Rechargeable Zinc/Sodium Vanadate Batteries with Enhanced Performance from Simultaneous Insertion of Dual Carriers, *Nat. Commun.*, 2018, **9**, 1656.

96 B. Tang, G. Fang, J. Zhou, L. Wang, Y. Lei, C. Wang, T. Lin, Y. Tang and S. Liang, Potassium Vanadates with Stable Structure and Fast Ion Diffusion Channel as Cathode for Rechargeable Aqueous Zinc-Ion Batteries, *Nano Energy*, 2018, **51**, 579−587.

97 X. Liu, H. Zhang, D. Geiger, J. Han, A. Varzi, U. Kaiser, A. Moretti and S. Passerini, Calcium Vanadate Sub-Microfibers as Highly Reversible Host Cathode Material for Aqueous Zinc-Ion Batteries, *Chem. Commun.*, 2019, **55**, 2265−2268.

98 L. Zhang, I. A. Rodríguez‐Pérez, H. Jiang, C. Zhang, D. P. Leonard, Q. Guo, W. Wang, S. Han, L. Wang and X. Ji, $ZnCl_2$ "Water-in-Salt" Electrolyte Transforms the Performance of Vanadium Oxide as a Zn Battery Cathode, *Adv. Funct. Mater.*, 2019, **29**, 1902653.

99 X. Wang, B. Xi, X. Ma, Z. Feng, Y. Jia, J. Feng, Y. Qian and S. Xiong, Boosting Zinc-Ion Storage Capability by Effectively Suppressing Vanadium Dissolution Based on Robust Layered Barium Vanadate, *Nano Lett.*, 2020, **20**, 2899−2906.

100 Y. Yang, Y. Tang, S. Liang, Z. Wu, G. Fang, X. Cao, C. Wang, T. Lin, A. Pan and J. Zhou, Transition Metal Ion-Preintercalated V_2O_5 as High-Performance Aqueous Zinc-Ion Battery Cathode with Broad Temperature Adaptability, *Nano Energy*, 2019, **61**, 617−625.

101 Z. Pan, J. Yang, J. Yang, Q. Zhang, H. Zhang, X. Li, Z. Kou, Y. Zhang, H. Chen, C. Yan and J. Wang, Stitching of $Zn_3(OH)_2V_2O_7{\cdot}2H_2O$ 2D Nanosheets by 1D Carbon Nanotubes Boosts Ultrahigh Rate for Wearable Quasi-Solid-State Zinc-Ion Batteries, *ACS Nano*, 2020, **14**, 842−853.

102 Y. Liu, C. Li, J. Xu, M. Ou, C. Fang, S. Sun, Y. Qiu, J. Peng, G. Lu, Q. Li, J. Han and Y. Huang, Electroactivation-Induced Spinel ZnV_2O_4 as a High-Performance Cathode Material for Aqueous Zinc-Ion Battery, *Nano Energy*, 2020, **67**, 104211.

103 C. Xia, J. Guo, Y. Lei, H. Liang, C. Zhao and H. N. Alshareef, Rechargeable Aqueous Zinc-Ion Battery Based on Porous Framework Zinc Pyrovanadate Intercalation Cathode, *Adv. Mater.*, 2018, **30**, 1705580.

104 L. Wang, K.-W. Huang, J. Chen and J. Zheng, Ultralong Cycle Stability of Aqueous Zinc-Ion Batteries with Zinc Vanadium Oxide Cathodes, *Sci. Adv.*, 2019, **5**, 4279.

105 C. Liu, Z. Neale, J. Zheng, X. Jia, J. Huang, M. Yan, M. Tian, M. Wang, J. Yang and G. Cao, Expanded Hydrated Vanadate for High-Performance Aqueous Zinc-Ion Batteries, *Energy Environ. Sci.*, 2019, **12**, 2273−2285.

106 Y. Liu, Q. Li, K. Ma, G. Yang and C. Wang, Graphene Oxide Wrapped CuV_2O_6 Nanobelts as High-Capacity and Long-Life Cathode Materials of Aqueous Zinc-Ion Batteries, *ACS Nano*, 2019, **13**, 12081−12089.

107 Z. Peng, Q. Wei, S. Tan, P. He, W. Luo, Q. An and L. Mai, Novel Layered Iron Vanadate Cathode for High-Capacity Aqueous Rechargeable Zinc Batteries, *Chem. Commun.*, 2018, **54**, 4041−4044.

108 L. Ma, N. Li, C. Long, B. Dong, D. Fang, Z. Liu, Y. Zhao, X. Li, J. Fan, S. Chen, S. Zhang and C. Zhi, Achieving Both High Voltage and High Capacity in Aqueous Zinc-Ion Battery for Record High Energy Density, *Adv. Funct. Mater.*, 2019, **29**, 1906142.

109 J. Zeng, K. Chao, W. Wang, X. Wei, C. Liu, H. Peng, Z. Zhang, X. Guo and G. Li, Silver Vanadium Oxide@Water-Pillared Vanadium Oxide Coaxial Nanocables for Superior Zinc Ion Storage Properties, *Inorg. Chem. Front.*, 2019, **6**, 2339−2348.

110 H. Jiang, Y. Zhang, L. Xu, Z. Gao, J. Zheng, Q. Wang, C. Meng and J. Wang, Fabrication of $(NH_4)_2V_3O_8$ Nanoparticles Encapsulated in Amorphous Carbon for High Capacity Electrodes in Aqueous Zinc Ion Batteries, *Chem. Eng. J.*, 2020, **382**, 122844.

111 J. Lai, H. Tang, X. Zhu and Y. Wang, A Hydrated $NH_4V_3O_8$ Nanobelt Electrode for Superior Aqueous and Quasi-Solid-State Zinc Ion Batteries, *J. Mater. Chem. A*, 2019, **7**, 23140−23148.

112 T. Wei, Q. Li, G. Yang and C. Wang, Highly Reversible and Long-Life Cycling Aqueous Zinc-Ion Battery Based on Ultrathin $(NH_4)_2V_{10}O_{25}{\cdot}8H_2O$ Nanobelts, *J. Mater. Chem. A*, 2018, **6**, 20402−20410.

113 H. Wang, M. Wang and Y. Tang, A Novel Zinc-Ion Hybrid Supercapacitor for Long-Life and Low-Cost Energy Storage Applications, *Energy Storage Mater.*, 2018, **13**, 1−7.

114 A. J. Perez, D. Batuk, M. Saubanère, G. Rousse, D. Foix, E. McCalla, E. J. Berg, R. Dugas, K. H. W. van den Bos, M.-L. Doublet, D. Gonbeau, A. M. Abakumov, G. Van Tendeloo and J.-M. Tarascon, Strong Oxygen Participation in the Redox Governing the Structural and Electrochemical Properties of Na-Rich Layered Oxide Na_2IrO_3, *Chem. Mater.*, 2016, **28**, 8278−8288.

115 Z. Wu, Y. Wang, L. Zhang, L. Jiang, W. Tian, C. Cai, J. Price, Q. Gu and L. Hu, A Layered $Zn_{0.4}VO_PO_4{\cdot}0.8H_2O$ Cathode for Robust and Stable Zn Ion Storage, *ACS Appl. Energy Mater.*, 2020, **3**, 3919−3927.

116 F. Wan, Y. Zhang, L. Zhang, D. Liu, C. Wang, L. Song, Z. Niu and J. Chen, Reversible Oxygen Redox Chemistry in Aqueous Zinc-Ion Batteries, *Angew. Chem. Int. Ed.*, 2019, **58**, 7062−7067.

117 Z. Liu, Q. Yang, D. Wang, G. Liang, Y. Zhu, F. Mo, Z. Huang, X. Li, L. Ma, T. Tang, Z. Lu and C. Zhi, A Flexible Solid-State Aqueous Zinc Hybrid Battery with Flat and High-Voltage Discharge Plateau, *Adv. Energy Mater.*, 2019, **9**, 1902473.

View Article Online
DOI: 10.1039/D0QM00577K

TOC :

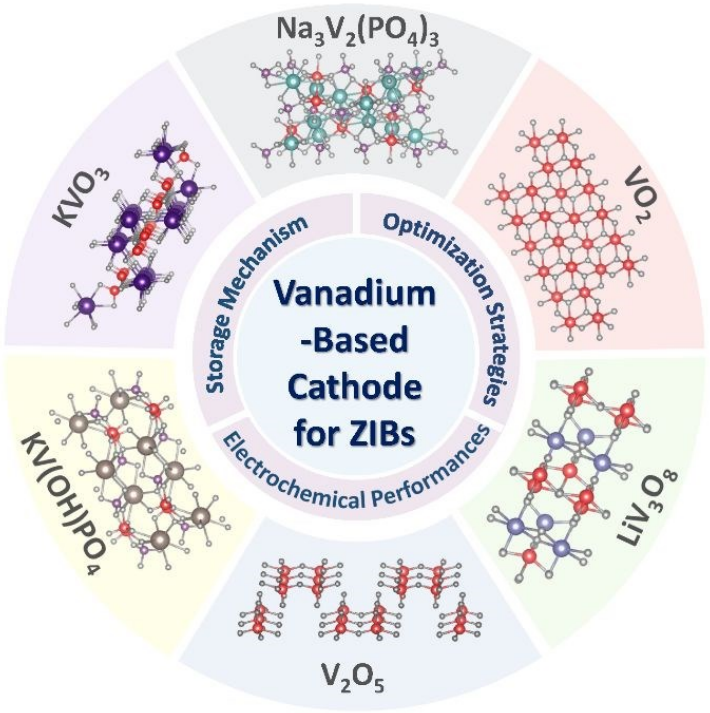

A comprehensive knowledge on the latest progresses of vanadium-based nanomaterials as well as the challenges and prospects for zinc ion batteries are reviewed.